Energy Storage Materials 64 (2024) 103075

Contents lists available at ScienceDirect

Energy Storage Materials

journal homepage: www.elsevier.com/locate/ensm

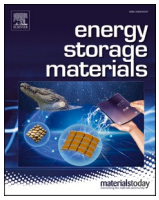

Recent advances in anode design for mild aqueous Zn-ion batteries

Ao Yu [a], Wei Zhang [a,b], Nimanyu Joshi [a,b], Yang Yang [a,b,c,d,e,*]

[a] NanoScience Technology Center, University of Central Florida, Orlando, FL 32826, USA
[b] Department of Materials Science and Engineering, University of Central Florida, Orlando, FL 32826, USA
[c] Renewable Energy and Chemical Transformation Cluster, University of Central Florida, Orlando, FL 32826, USA
[d] Department of Chemistry, University of Central Florida, Orlando, FL 32826, USA
[e] The Stephen W. Hawking Center for Microgravity Research and Education, University of Central Florida, Orlando, FL 32826, USA

ARTICLE INFO

Keywords:
Zinc-ion batteries
Material design
Zn anode protection
Intercalated anode

ABSTRACT

Rechargeable aqueous zinc-ion batteries (ZIBs) are promising as a competitive candidate to replace the dominant lithium-ion batteries due to fewer safety concerns, simplified operational conditions, abundant resources, and cost-effectiveness. However, as anode material, zinc metal suffers from the inevitable zinc dendrites growth, hydrogen evolution reaction (HER), and inherent corrosion in aqueous electrolytes, which severely restrict the reliability of ZIBs. To realize the commercialization of ZIBs, various strategies such as the design of protective coating layers, host materials for zinc stripping/plating, and intercalated anode materials, were developed to overcome the inherent limitations of zinc metal. A thorough understanding of the structure-performance relationship is required for the development of efficient anodes for ZIBs. This review aims to provide a comprehensive overview of the research progress of ZIB anodes concerning protective coating layers on zinc surfaces and intercalated anode materials due to different zinc storage mechanisms. First, the limitations of zinc metal anode and intercalated anode materials are summarized. Second, A summary of diverse strategies and advancements in protective coating layers design for zinc anode is presented. Third, the rarely reported intercalated anode materials are also discussed based on their storage mechanisms, materials specifications, and limitations. Finally, the potential research directions and strategies for developing a high-performance anode for ZIBs were proposed to offer insights into future research endeavors.

1. Introduction

Continuous global power consumption heavily relies on the burning of non-renewable and highly polluting fossil fuels. This presents a significant worldwide challenge that demands our attention. An urgent requirement for transforming the unsustainable and contaminative energy supply to renewable and eco-friendly alternatives remains a critical concern. Currently, a range of clean energy sources, such as solar and wind energy, have gained widespread adoption [1], which are captured and converted into renewable electricity, thus fulfilling a substantial portion of industrial power requirements. However, the transportation and storage of electricity present numerous challenges encompassing storage capacity, dependability, expenses, safety, ecological concerns, and transmission spans. As a result, ensuring a sustainable and reliable energy supply heavily relied on establishing a secure and solid energy storage mechanism. Nowadays, lithium-ion batteries have emerged as the leading technology for rechargeable energy storage solutions. However, the inevitable utilization of flammable organic electrolytes, highly active lithium utilization, the scarcity of lithium resources, and the elevated expenses substantially hinder its extensive implementation. Nonetheless, rechargeable aqueous zinc-ion batteries (ZIBs), which offer reduced safety concerns, simplified operational conditions, abundant resources, and enhanced cost-effectiveness, holding the capacity to effectively surmount the inherent limitations of lithium-ion batteries, ensuring an enormous potential for widespread adoption. Furthermore, zinc metal possesses a notable specific capacity (820 mAh g^{-1}) [2,3], surpassing that of lithium metal in volumetric capacity [4]. Compared to the other active metals (such as Li, Na, K, Ca et.al), zinc can be employed directly as the anode due to its inherent resistance to oxidation in aqueous electrolyte [5], the rational redox potential of −0.76 V vs. standard hydrogen electrode (RHE), and reversible conversion of Zn/Zn^{2+} in aqueous electrolytes.

For the aqueous ZIBs, the performance of the zinc anode is highly dependent on the pH of the electrolytes. The zinc metal in acidic

* Corresponding author.
E-mail address: Yang.Yang@ucf.edu (Y. Yang).

https://doi.org/10.1016/j.ensm.2023.103075
Received 13 November 2023; Accepted 15 November 2023
Available online 22 November 2023

electrolytes is unstable due to the direct reaction with zinc. Moreover, in the alkaline electrolyte, the Zn anode suffers from a solid-solute-solid (ZnO-$Zn(OH)_4^{2-}$-Zn) process. The generated ZnO deactivates the zinc surface, resulting in the low utilization of active zinc. The chemical reactions of zinc anode in the alkaline electrolyte can be elucidated as follows [6]:

$$Zn + 4OH^- \leftrightarrow Zn(OH)_4^{2-} + 2e^-$$

$$Zn(OH)_4^{2-} \leftrightarrow ZnO + H_2O + 2OH^-$$

In a neutral electrolyte, the reaction on the zinc anode is listed below:

$$Zn \leftrightarrow Zn^{2+} + 2e^-$$

Since the discovery of Zn-MnO_2 batteries in mild 2 M $ZnSO_4$ in the 1980s, extensive investigations have been conducted for ZIBs in mild electrolytes [7,8]. It has been proved that mild electrolytes can eliminate the ZnO-triggered passivation and endow a relatively high reversibility of zinc plating/stripping to alleviate the dendrite growth of zinc [9]. Despite the numerous benefits associated with the zinc anode in mild electrolytes, it remains confronted with three primary challenges: zinc dendrite growth and proliferation, HER, and corrosion resistance of zinc. The undesirable growth of dendrites in ZIBs can lead to the detachment of these structures from the zinc anode, leading to "dead zinc" generation, which diminishes the effective capacity and coulombic efficiency (CE) of the anode. Moreover, the growth of zinc dendrites has the risk of piercing the membrane, causing a short circuit that impedes the battery's extended cycling capability. Additionally, within a mild electrolyte, the HER occurring on the exposed zinc surface can lead to continuous electrolyte consumption and zinc corrosion. The consequent production of hydrogen gas further elevates the internal pressure of the battery, ultimately culminating in electrolyte leakage.

To circumvent the three problems of zinc anode, constructing a highly stable Zn anode with various strategies was fully explored. One of the most effective methods is to construct a protective coating layer on the bare zinc surface, which can optimize the ion diffusion, and zincophilicity between the protective layer and Zn^{2+}, distributed concentration as well as local electrical field [1]. The protective layers on the zinc surface prevent the direct contact of zinc and electrolyte, effectively preventing the zinc anode from corrosion. Furthermore, the rational design of the protective layer including structure and physical-chemical characteristics can not only induce the zinc deposition but also suppress the HER, which is beneficial for extending the stability and shelf-life of the zinc anode. For example, a Nafion-Zn-X protective layer possessing proper ion tunnels can selectively allow Zn^{2+} transportation in the coating layer, while the other ions such as the SO_4^{2-} and hydrated Zn^{2+} are prevented. Such selective ion diffusion results in a redistribution of the concentration field and directional ion migration, which can effectively suppress the 2D diffusion of Zn^{2+} [10]. In addition, the zinc nucleation process is also crucial to zinc growth, which is greatly affected by the zincophilicity between the protective layer and Zn^{2+} determined by the energy barrier of zinc deposition. For example, introducing a zincophilic surface can reduce the nucleation energy barrier [11,12], thus facilitating the zinc nucleation on the surface of the zinc anode. In addition, some protective coating layers with certain surface structures can optimize the surface distributed electrical field by decreasing the local current density, and finally realize a uniform zinc deposition [13,14]. According to the equation: $\tau = \pi D \frac{eC_0(\mu_a+\mu_{Zn^{2+}})^2}{2J\mu_a}$, decreasing the local current density can prolong the duration time when Zn dendrite begins to emerge [14]. Where τ, D, C_0, μ_a, μ_{Zn}^{2+}, J, and e present the time when zinc dendrites begin to emerge, diffusion coefficient, original concentration of electrolyte, anionic mobility, Zn^{2+} mobility, local current density, and electronic charge, respectively. Based on this equation, a protective coating with a larger specific surface area can effectively lower the local current density, which is beneficial to relieve the dendritic growth of zinc. Therefore, the 2D and 3D coating layers with large specific surface areas such as graphene, MXene, porous alloys, and metal-organic frameworks (MOFs) are constructed on the zinc surface [12,15-17]. While the majority of studies concentrate on developing effective protective layers for zinc surfaces, there is also significant interest in employing host materials that have three-dimensional (3D), porous, or ordered structures as anodes for zinc-ion batteries (ZIBs). This approach involves preloading a zinc source onto the host materials, instead of using a zinc sheet directly as an anode. Generally, these host materials are either coated onto non-zinc substrates or used directly as host substrates for zinc preloading, subsequently serving as anodes in zinc-ion batteries (ZIBs). The absence of a zinc sheet in the anode configuration substantially reduces zinc usage, which in turn significantly increases the depth of discharge (DOD). These types of host materials and their implications for ZIBs will be comprehensively discussed in Section 3.2., titled "The design of host materials for ZIBs anode".

Another alternative strategy is to develop an intercalated anode for ZIBs, which does not contain metallic zinc. The energy storage/release is achieved by the reversible Zn^{2+}insertion/extraction or redox reactions involving the $Zn^{2+}$and functional groups. Regarding the Zn^{2+}insertion/extraction typed intercalation anode materials of ZIBs, they predominantly comprise the inorganics with layered structures. These accessible layered structures should possess sufficiently large interlayer to accommodate Zn^{2+} and provide the ionic channels for Zn^{2+} transportation, and keep the integrity even after ample Zn^{2+} insertion/extraction. In contrast, the redox reaction typed intercalation anode materials of ZIBs typically involve organics with active functional groups capable of coupling with Zn^{2+}. Therefore, in such intercalated anode materials, the layered structures with ion channels and surface active groups to capture Zn^{2+} are crucial to the overall performance. Some inorganic and organic intercalated anode materials for ZIBs are developed, for example, the Chevrel phase Mo_6S_8 [18,19], poly 3,4,9,10-perylentetracarboxylicdiimide, PPTCDI [20]. Taking the Mo_6S_8 as an example, during the charge/discharge process, the intercalated anode materials experience the phase transformation: $Mo_6S_8 \leftrightarrow ZnMo_6S_8 \leftrightarrow Zn_2Mo_6S_8$ due to the Zn^{2+} insertion and extraction [18]. However, the specific capacity and storage mechanism of most intercalated anode materials is still limited and unclear due to insufficient work reported.

Therefore, in the pursuit of developing suitable anodes for ZIBs in mild aqueous electrolytes, it becomes crucial to comprehend the storage mechanisms and challenges associated with various anode types. Gaining a comprehensive understanding of the ongoing research progress will enable us to grasp the most recent and optimized strategies. While numerous published reviews concerning ZIB anodes have predominantly concentrated on modifying the zinc anode, it is essential to note that a multitude of innovative strategies for anode design extends beyond solely focusing on zinc metal. Notably, other anode materials including host materials that do not directly employ zinc sheets, as well as intercalated anode materials, play equally crucial roles. To date, a thorough comparison and understanding of these three distinct research areas remain seldom reviewed. Specifically, a systematic classification of the differing working mechanisms and structural characteristics is rare. Consequently, a comprehensive understanding of anode materials for zinc-ion batteries (ZIBs) is essential for furthering the development and advancement of this field. In this review, a comprehensive summary of the recent achievements of the anode materials for ZIBs in mild electrolytes is presented. It contains the critical challenges associated with metallic zinc anodes for ZIBs that need to be addressed ultimately, including the dendrite growth of zinc, HER, and zinc corrosion, and the corresponding decay mechanisms and solutions. In addition, effective strategies of preparing host materials as zinc anode was given and emphasized their differences from the metallic zinc anodes, aiding in differentiating two similar strategies and identifying novel research directions. Furthermore, the storage mechanisms of the two different types of intercalation anode materials for ZIBs (including the inorganics and

or organics) and the basic fundamental requirements for developing high-performance intercalation anode materials for ZIB are systematically reviewed.

2. Main challenges of anode materials for mild aqueous ZIBs

2.1. Challenges of zinc anode

In the zinc plating/stripping process, the chemical reactions take place at the electrolyte/electrode interface, where the zinc dendrites grow, the passivation layer is generated, and HER takes place. During the zinc plating process, the zinc tends to grow primarily at the tip sites and the area where the dendrites are already present, finally resulting in the formation of a sharp and loose structure (Fig. 1**a**). The sharp zinc dendrites can easily pierce the membrane and trigger a short circuit once the zinc dendrites contact the cathode. Furthermore, the loose structure of zinc dendrites is easily removed from the zinc anode to generate "dead zinc", which reduces the capacity and CE of the zinc anode. The ion diffusion, distributed electric field, and current density have great effects on the dendrite growth of zinc. It is inevitable to cause the concentration gradient from the interface to the bulk electrolyte during the plating process. The Zn^{2+} concentration near the anode surface is lower than the bulk electrolyte due to continuous consumption of the Zn^{2+} and limited Zn^{2+} diffusion, which in turn results in an increase of overpotential on the surface of the zinc anode. Such overpotential would seriously destroy the uniformly distributed electric field and further result in coarse zinc deposition [13]. The current density also directly affects the zinc deposition. In general, high current density has more intense effects on the dendrite growth of zinc than low current density [21]. Therefore, creating an anode with a large specific surface area proves advantageous in achieving low current density, which facilitates uniform zinc deposition via generating a stable current density field and a uniformly distributed electric field [22,23]. Furthermore, the zinc deposition is also related to the intrinsic characteristics of the host materials (for example, lattice parameters and zincophilicity). It has been confirmed that graphene can induce parallel and uniform zinc deposition due to the similar lattice parameter between zinc and graphene [24].

The HER and zinc corrosion take place simultaneously during the charge/discharge process (Fig. 1**b-c**), For full ZIBs, during the discharge process, Zn loses two electrons to form Zn^{2+}, while the H^+ may capture electrons to generate H_2. During the charging process, hydrogen evolution is a competitive reaction to the reduction of Zn^{2+}, which reduces the CE and consumes the Zn^{2+}. When the H_2 is released from the splitting of H_2O, the concentration of OH^- increases (namely, increases the pH of the electrolyte). The amount of the OH^- would combine with Zn^{2+} to form $Zn(OH)_4^{2-}$. Once the $Zn(OH)_4^{2-}$ reaches saturation, the insulated and passivated ZnO would generate and adhere to the zinc surface [25], which increases the electrical resistance and reduces the CE of plating/stripping [26–28]. Furthermore, the generated H_2 can also increase the inner pressure of a battery, potentially leading to an electrolyte leakage and battery malfunction. Therefore, the construction of a proper protective coating layer on the zinc surface to restrain the HER and zinc corrosion is of great significance in improving the stability of zinc anodes.

2.2. Challenges of intercalated anode

To mitigate the problems of the direct use of zinc as an anode for ZIBs, a promising strategy to avoid those problems is to develop zinc-free anode materials, namely intercalated anodes (Fig. 1**d**), Currently, few explorations about intercalated anode materials for ZIBs are reported due to the limited choice of intercalated materials. Furthermore, the sluggish kinetics of Zn^{2+} intercalation into the layer spacing restricts ionic diffusion and charge transfer in the active materials [9], which results in a higher diffusion energy barrier and is harmful to the storage performance. Although a material with larger layer spacing can accelerate the Zn^{2+} kinetics and improve the intercalation/deintercalation process, the highly extended layer spacing makes the materials fragile, which means long cycling would disable the integrity of the materials [9]. On the other, intercalated anode materials submerged in a mild electrolyte experience unavoidable dissolution, occurring throughout the repetitive charge and discharge cycles. These anode materials undergo both chemical and structural alterations, resulting in the dissolution of active components into the electrolyte and ultimately causing a substantial reduction in their capacity [29]. Currently, one of the biggest challenges for the intercalated anode in ZIBs is the low energy density due to relatively low capacity and the storage mechanism is still unclear for many intercalated anode materials [1]. Nowadays, intercalated anode materials are mainly focused on chalcogenides and a few organics [30], the limited quantity of which seriously restricts the further exploration of intercalated anode materials. To achieve an intercalated anode material with high performance, it should possess high specific capacity, excellent stability and rate performance, and low zinc insertion potential vs. Zn/Zn^{2+}.

3. Design strategies for ZIBs anode

3.1. The design of protective coating on zinc anode

Bare zinc foil has been proven to act as an anode for ZIBs, however, it is unreasonable to use zinc directly due to the easily formed zinc dendrites on the electrolyte/electrode interface. Regulating the interfacial characteristics has evident effects on the formation of dendrites. An effective coating layer is characterized by poor electronic conductivity, excellent ionic diffusivity, and chemical/mechanical stability [13,31,32], ensuring the unimpeded flow of zinc ions concomitant with the prevention of electron-induced short-circuiting, and enhanced adhesion

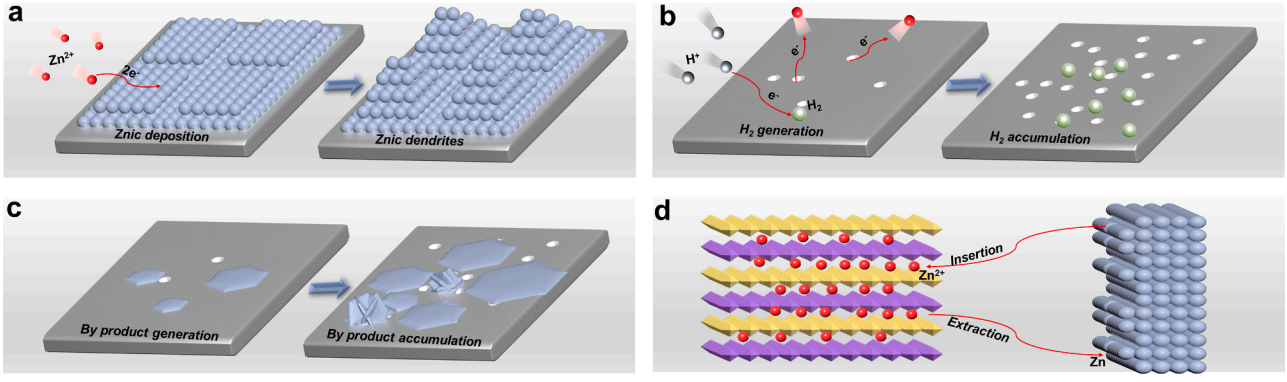

Fig. 1. (a-c) Challenges to zinc metal anode (d) Storage mechanism of intercalated anode materials of ZIBs.

to zinc surface. Zinc is the one with high chemical activity, which has a theoretical reduction potential of −0.762 V vs. RHE (lower than that of the H_2 evolution potential of 0 V vs. SHE). Such lower potential implies the HER is always accompanied by zinc plating. This side reaction of H_2 evolution indeed causes low energy efficiency, leakage of electrolytes, and safety problems due to the increased inner pressure. A protective coating layer can separate the direct contact between the active zinc and electrolyte, creating a stable interface for zinc deposition and suppressing the H_2 evolution.

The objective in applying protective coatings to zinc anode for ZIBs is to establish a coherent layer characterized by robust adhesion to the zinc substrate, coupled with an outstanding capacity to prevent delamination that caused by volumetric alterations or gas evolution during the electrochemical cycling of zinc (**Table S1**). To build an integrated layer and enhance the adhesion to the zinc surface, the surface treatment of the zinc surface and optimization of the coating layer should be purposely designed. Preparatory treatments of the zinc anode surface, for example, chemical etching, polishing, or electrochemical activation to remove oxides or contaminants can effectively bolster the natural adhesion for subsequent protective layers. In addition, interfacial layers that exhibit strong bonding characteristics to both the zinc anode and the overlying protective layer can enhance adhesion. For example, the ZnO adhesive to the zinc surface can be used as an intermediate to link the MOF coatings and the zinc substrate [33]. Crucially, the artificial design of the coating layer plays a predominant role in contributing to this issue. The incorporation of nanostructuring within the protective layer significantly enhances the contact surface area and mechanical interlocking, thereby facilitating improved adhesion. In addition, the configuration of the protective layer should be conceptualized to include stress-releasing characteristics, such as a composition that exhibits a gradual or stratified transition from the interface to the exterior surface.

The protective coating layer on the zinc surface may suffer from inevitable volume changes due to the plating/stripping of zinc, potentially resulting in the detrimental exfoliation of the coating. This necessitates a focus on the malleability of materials and adept stress management. The use of elastic or flexible coatings, such as elastomeric polymers [34–36] or composite 2D materials [15,16,37] that combine conductivity with flexibility, is essential. These materials are integral to maintaining layer integrity by withstanding mechanical deformation. Additionally, design features implemented for stress alleviation, such as microscale trenches or porous structures within the coating, act as expansion joints and can absorb stress caused by anode expansion. Another method to prevent exfoliation is to promote uniform deposition of zinc on the surface of the coating rather than embedding zinc within the coating layer itself. In parallel, addressing the challenge of gas evolution entails both chemical strategies and design alterations. The development of a stable and homogeneous coating layer inert to the HER can curtail gas generation and accommodate volumetric changes in the coating layer. The creation of coatings with channels and a porous structure allows for the safe release of gases, preventing the buildup of pressure that might cause blistering or delamination.

Various protective coating layer materials demonstrate different effects on optimizing the zinc anode performance. Regarding the protective coating layer on the zinc surface, it is composed of inorganic metal/non-metal oxides, organic polymers, organic/inorganic composites, 2D carbon-based coating layers (such as graphite and graphene), 2D Mxenes, alloys, and their composites (**Table S1**).

3.1.1. Inorganic metal/nonmetal compounds-based coating layer

The most common inorganic metal/nonmetal compound modification layers, including nano-SiO_2, porous $CaCO_3$ [38], Al_2O_3 [39], CeO_2 [40], $BaTiO_3$ [41], amorphous TiO_2 [42], ZrO_2 [43], ZnS [44], ZnF_2/Ag [45], ZnP [46] and ZnSe [47] have been explored for protecting the zinc anode in ZIBs. Those protective coating layers on the zinc surface can separate the direct contact of zinc metal and electrolyte, which protects the anode from corrosion and alleviates the HER. In addition, they also exhibit different zincophilic characteristics and wettability that can further regulate the Zn^{2+} diffusion by controlling the electrolyte flux, which would be beneficial for zinc deposition. Constructing appropriate inorganic metal/nonmetal composites on the zinc surface can significantly improve the anode lifespan. The porous $CaCO_3$ induces a bottom-up growth of zinc by guiding the homogeneous electrolyte flux and confining the zinc plating (Fig. 2**a**) [38]. By introducing an inert ZrO_2 layer on the surface of zinc, a physical barrier was constructed to separate the direct contact of zinc and electrolyte, thus promoting the corrosion resistance and suppressing the H_2 evolution as well as de-accelerating the formation of a robust ZnO layer (Fig. 2**b**) [43]. In general, the formed ZnO layer adhered to the zinc during the plating and stripping would impair the zinc deposition, which leads to low coulombic efficiency as well as capacity fade [48,49]. It would be better to impede the formation of ZnO for ZIBs, while it is also advantageous to note that ZnO also reduces the desolvation barrier and has good zincophilic characteristics. Such properties endow the uniform zinc deposition/dissolution by promoting the Zn^{2+} reaction kinetics [50–53]. Recently, a ZnO coating layer on zinc foil was in situ fabricated using an iodine-assisted strategy. As shown in Fig. 2**c,** iodine dispersed in water was firstly dropped on the zinc surface to generate unstable zinc iodide ($Zn + I_2 \rightarrow ZnI_2$), then the generated ZnI_2 reacted with oxygen to form ZnO, and finally forming a ZnO interface layer on the Zn anode (named as IAZO) [54]. The whole process only takes 5 min. The XRD of the IAZO displayed the main peaks for zinc and extremely small peaks for ZnO, indicating only a small amount of ZnO was formed after I_2 treatment. Meanwhile, the enhanced ZnO peaks in the XPS curves confirmed the increased ZnO content compared to the bare zinc. The activation energy of IAZO was proved lower than that of the bare zinc, demonstrating the desolvation energy was reduced after introducing ZnO layer, which implied a reduced solvent sheath effect and enhanced transportation kinetics of Zn^{2+} [55,56]. Furthermore, the stronger binding between Zn^{2+} and different ZnO sites (c-O, −1.46 eV; f-O, −4.88 eV) compared to that of bare zinc (−0.25 eV) indicates the Zn^{2+} has better affinity with ZnO, resulting in a positive constrained local zone for the reduction of Zn^{2+} to Zn^0. For the surface of bare zinc, the Zn^{2+}prefers to migrate quickly to the nucleation sites due to the weak interaction within the metallic zinc and gradually facilitates the dendrites growth. Benefiting from the reduced desolvation barrier and optimized Zn^{2+} affinity of the ZnO coating layer, the symmetrical cell assembled with IAZO can be stably operated over 3100 h. Another interesting work pointed out that the zinc metal and oxides coating layer (CeO_2, MoO_3, WO_3, and TiO_2) can result in a physical barrier, which can suppress the pernicious side reactions. Due to the disparities in work functions between the zinc and oxides, interfacial ohmic contacts are established between the zinc and oxide semiconductors. This discrepancy induces a flow of electrons from the metallic zinc towards the oxides, resulting in the formation of an electron-enriched region at the interface with the metal oxides, referred to as the "anti-blocking layer". The appropriate work function difference between CeO_2 and Zn facilitates improved diffusion kinetics for Zn^{2+} and diminishes the nucleation barrier for Zn, thereby promoting a dendrite-free deposition of Zn. Concurrently, the CeO_2 layer serves a protective function, significantly mitigating corrosion and the HER [40]. In addition to the inorganic coating composites, the organic and inorganic composite was also developed. Recently, an inorganic nanolayer (TiO_2) and organic molecule (steric acid, SA) layer are self-assembled on the surface of a zinc sheet to construct Zn@SA@TiO_{2-}. The deliberately constructed SA acts as the hydrophobic layer to impede the H_2O splitting and the TiO_2 can strongly bond to OH^-, thus resulting in an accelerated Zn^{2+}, good corrosion resistance and suppressed HER, and dendrite-free zinc growth [57].

The inorganic metal/nonmetal compound-based coatings for zinc anodes undoubtedly play a positive role in improving the overall performance of the zinc anode. However, their disadvantages cannot be ignored. These include brittleness and lack of flexibility, weak adhesion to the zinc surface, and limited self-healing capability. Typically, most

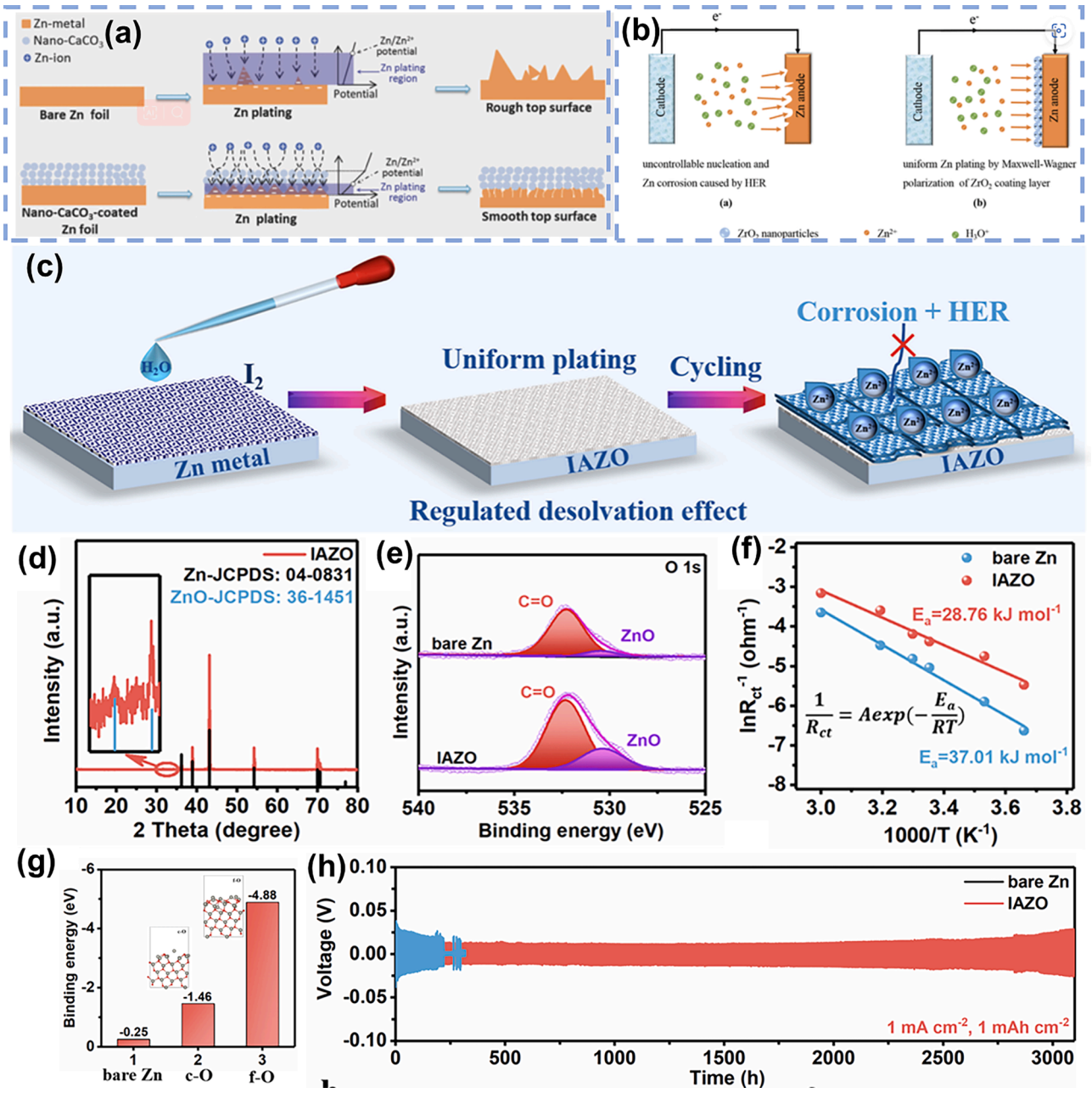

Fig. 2. (a) Illustrations of zinc deposition on bare and nano-$CaCO_3$-coated Zn foils. Reproduced from Ref. [38]. Copyright (2018) Wiley-VCH GmbH. (b) Zinc stripping/plating processes on bare Zn anode and ZrO_2-coated Zn anode. Reproduced from Ref. [43]. Copyright (2020) Wiley-VCH GmbH. (c) Illustration of ZnO coating process on bare Zn foils. (d) XRD and (e) XPS of bare Zn and IAZO. (f) The Arrhenius curves and corresponding activation energies. (g) The adsorption energy of Zn^{2+}at different adsorption sites on bare Zn and ZnO. (h) Cycling curves of symmetric cells at 1 mA cm^{-2} (1 mAh cm^{-2}). Reproduced from Ref. [54]. Copyright (2023) American Chemical Society.

inorganic metal/nonmetal compounds can only be applied to the zinc surface using physical methods (such as doctor blade coating and drop coating), which may result in a weak interface. These shortcomings present significant challenges in balancing the protective advantages against the potential drawbacks of using inorganic compound-based coatings for zinc anodes in ZIBs.

3.1.2. Organics-based coating layer

Organics-based protective coating layers on zinc foil possess good flexibility that can withstand the cycling volume change. Meanwhile, the organic coatings were used as molecular brushes on the surface of metals and the ultra-small distance between the brush can provide sufficient channels for ion transportation and metallic normalization deposition [58,59]. Furthermore, some of the zincophilic surficial functional groups (eg. Sulfo, hydroxyl, and N-acetylamino groups [59, 60]) or hydrophilic functional groups (eg. Amide [61]), can redistribute the ion concentration and reduce the hydrated Zn^{2+} desolvation energy [59]. An organic poly-(anionic 3-sulfopropyl methacrylate potassium salt) (PSPMA) molecular brush terminating with sulfo groups on the zinc surface was purposely designed for uniform zinc deposition (Fig. 3**a-j**). Upon exposure to UV radiation, the photosensitive amine groups in polydopamine (PDA) are activated and then generate abundant amine radicals, resulting in the polymerization of PSPMA. After introducing PSPMA, the contact angle is greatly reduced from 85° to 5° and the corresponding wetting free energy increased from 0.15 J mol^{-1} to 1013 J mol^{-1}, which demonstrates the sulfo-terminated PSPMA molecular

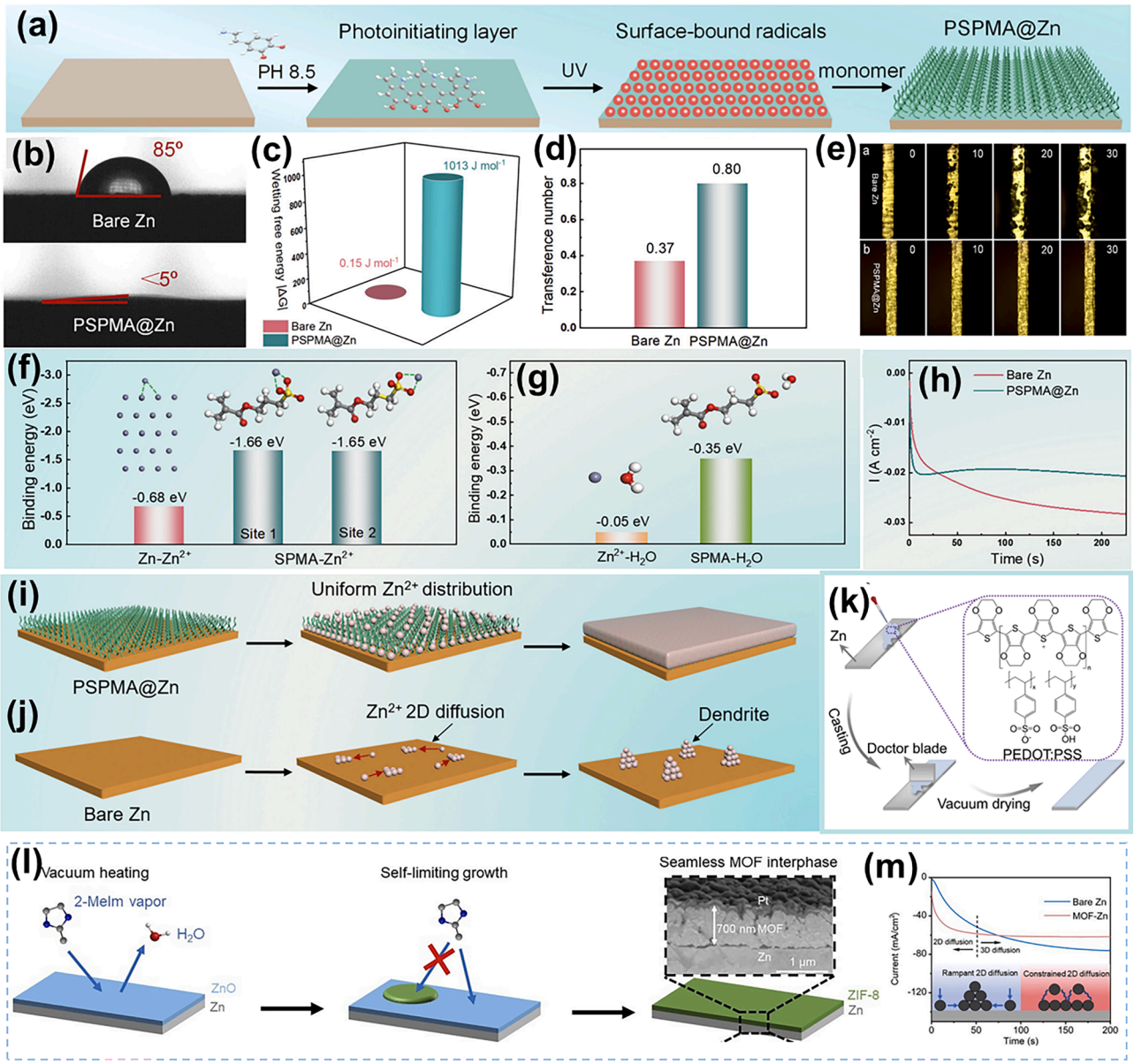

Fig. 3. (a) Illustration of in situ coating of organic PSPMA on zinc. (b) Contact angle test on the surface of bare zinc and PSPMA@Zn, and corresponding (c) wetting free energy and (d) transference number. (e) In situ optical monitoring of the zinc deposition process on bare zinc and PSPMA@Zn after operating 50 cycles at 1 mA cm^{-2}. Theoretical modes and binding energy of (f) $Zn^{2+}$and (g) H_2O on the surface of bare zinc and PSPMA@Zn. (h) I–t curves of bare Zn and PSPMA@Zn electrodes at the voltage of −150 mV. Illustration of zinc deposition on the surface of (i) PSPMA@Zn and (j) bare zinc. Reproduced from Ref. [59]. Copyright (2023) Royal Society of Chemistry. (k) Illustration of the fabrication of PEDOT: PSS@Zn electrode. Reproduced from Ref. [36]. Copyright (2023) American Chemical Society. (l) Illustration depicting the construction of MOF on a bare zinc surface. Reproduced from Ref. [33]. Copyright (2023) Elsevier.

brushes enhance the wettability and, meanwhile, facilitate Zn^{2+} diffusion [34,35]. The enhanced transference number further confirmed the optimized Zn^{2+} diffusion kinetics state. In a typical symmetrical cell, the dendrites start to form on the surface of the bare zinc electrode at 10 min (current density = 10 mA cm^{-2}), while the PSPMA-coated zinc remains flat without any dendrites. The DFT calculation indicated the sulfo-terminated PSPMA coating has higher binding energy with Zn^{2+} than that of the bare zinc, demonstrating the hydrated Zn^{2+} has a stronger interaction with the sulfonate groups. Furthermore, the Zn^{2+} in H_2O solvent is in the form of hydrated Zn^{2+} ($[Zn(H_2O)_6]^{2+}$), which means the desolvated ability of the electrolyte/anode interface is crucial to the following zinc deposition [62]. The stronger binding energy with H_2O indicates the solvent shell structure of hydrated Zn^{2+} is sufficiently weakened by absorbing the solvent molecular, thus leading to a low desolvation energy of the PSPMA@Zn anode. The chronoamperometry (CA) curves in Fig. 3**j** imply a 2D diffusion and nucleation process of bare zinc, which results in uneven dendrites growth; while for the PSPMA@Zn anode, it is a typical homogeneous 3D diffusion and nucleation process, facilitating smooth zinc deposition process. Such different 2D and 3D diffusion of Zn^{2+} result in the complete zinc deposition behavior on bare zinc and PSPMA@Zn. Recently, a type of organic polymer of poly(3,4-ethylenedioxythiophene): poly-(-styrenesulfonate) (PEDOT: PSS) has been confirmed as an effective coating layer for enhancing the zinc anode stability [36]. As shown in Fig. 3**k**, the integrated PEDOT: PSS@Zn composite anode was prepared via a simple doctor blade coating. The results indicated the surface PEDOT: PSS induced the zinc growth direction of (002). The C—C bond in the thiophene and the sulfur-based functional groups can react with the Zn^{2+}, greatly promoting the nucleation and growth of zinc.

Most organic-based coating layers have difficulty in recyclability and

biodegradability, biomass-derived organics are also good choices for creating a protective coating layer on the zinc surface. For example, biomass chitosan and poly-aspartic acid not only can be recycled and biodegraded but also can be easily obtained from nature. Furthermore, the abundant zincophilic functional groups (hydroxyl and N-acetylamino groups) on the chains of chitosan can reduce the desolvated energy barrier and endow a uniform zinc deposition, and the poly-aspartic acid can buffer the proton in the electrolyte and further weaken the HER and side reactions [60]. The Zn^{2+} solvation is also affected by the metal-organic-framework (MOF) coating layer due to the angstrom-sized pore [33,63,64]. For example, as shown in Fig. 3**l**. The 2-methylimidazole (2-MeIm) used to construct ZIF-8 can directly react with the initial ZnO passivation layer on the Zn surface through a deprotonation effect. Simultaneously, it forms a dense crystalline porous MOF on the zinc surface by coordinating with Zn^{2+} [33]. The zinc deposition on ZIF-8 decorated zinc displays a shortened 2D diffusion process and a dominated 3D diffusion process.

Actually, the organics were not only used as the modified layer alone, an amazing work found the organic (polyacrylonitrile, PAN) decorated with a dielectric substance (silicon nitride, Si_3N_4) can regulate the dielectric property of the electrode/electrolyte interface, which could effectively modify the affect deposition/dissolution of zinc [65]. In such a PAN/Si_3N_4 (PSN) composite layer, PAN film protects the Zn from being corroded through blocking the H_2O/O_2, while the high dielectric Si_3N_4 accelerates the ion transportation and induces the uniform zinc deposition. In addition, it was found that the additives in PAN with higher dielectric constant could further optimize the performance of the protective layer when replacing the amorphous Si_3N_4 with lower dielectric SiO_2 and β-Si_3N_4.

Organic coatings are endowed with exceptional elasticity and the capacity for selective ion transport within the electrolyte, which contributes to the augmented performance of the zinc anode. Nevertheless, the mechanical robustness of such organic coatings requires enhancement. Furthermore, further development is needed to optimize surface functional groups for selective ion conduction and refine molecular architectures, aiming at bolstering the stability of the zinc metal anode.

3.1.3. 2D carbon/MXene-based coating layer

In addition to the inorganic metal/nonmetal oxides that can promote zinc stability, Layered two-dimensional (2D) carbon-based materials, including graphite [66,67], graphene [15], graphdiyne [37], and carbonitride [68] can effectively suppress the dendrites growth by tuning the deposition direction of the byproduct and homogenizing the distribution of the electrical field. The 2D carbon-based coating layer, with its large specific surface area, can disperse a portion of the anode's electronic charge and possesses abundant surface defects. These defects result in high electrochemical activity, providing numerous nucleation sites for zinc deposition and significantly reducing the local current density. In essence, a highly conductive and uniform 2D materials coating layer can equalize the distributed electric field and stabilize the zinc plating process on the anode's surface. [66,69]. A pencil drawing layered graphite with high conductivity on zinc substrate was successfully developed, which not only has an extremely low graphite mass loading of 0.18 mg/cm^2, but also displayed enhanced durability compared to the bare zinc foil and commercial graphite coated zinc foil [67]. After loading the graphite (the sample was named Zn-G), the corrosion resistance of Zn-G is greatly enhanced. As shown in Fig. 4**a**, the surface of bare zinc is severely corroded, while the Zn-G retains its original surface. In addition, the process of friction reduced the graphitization degree of pristine graphite and increased the surface defects, thus ensuring more exposed nucleation active sites for zinc and overpotential reduction. The symmetrical Zn-G//Zn-G cell has a lower overpotential of 28 mV and can work stably over 200 h (Fig. 4**b**), which is better than that of the bare zinc and commercial graphite-coated zinc (Zn-CG). One can see that new peaks of $Zn_4(OH)_6SO_4{\cdot}H_2O$ appear on bare zinc after a long cycling test but not on the Zn-G, indicating the graphite coating layer can effectively hinder the growth of byproducts and dendrites. Furthermore, because of the low Young's modulus of the graphite layer, it can act as a soft buffer layer for Zn^{2+} migration and cover the stepped zinc surface to homogenize the local distributed electrical field, which was further confirmed by the simulated calculations in Fig. 4**e-f**. Because of the sufficient nucleation sites, low Young's modulus as well intrinsic high conductivity, the Zn^{2+} prefers to be absorbed onto the defect sites and deposited on the layer of graphite, endowing the uniform zinc deposition on the surface of Zn-G.

Zinc deposition is a diffusion-controlled process that is affected by the combined action of the electric field and distributed concentration gradients [70]. Besides the local electrical field distribution that affects the zinc deposition, the interfacial ion concentration distribution, which can influence the ion transportation and interfacial reaction, is also important. The concentration distribution is related to the type and size of ions as well as the interface layer characteristics (e.g., selective to different ions and porosity). In a mild aqueous electrolyte, the dissolved Zn^{2+} takes the form of hydrated Zn^{2+} ($[Zn(H_2O)_6]^{2+}$), indicating that Zn^{2+} is encompassed by six H_2O molecules. This results in a larger ion diameter of 4.3 Å than that of the Zn^{2+}(0.74 Å) [71]. The surrounding H_2O molecules impair the desolvation of $[Zn(H_2O)_6]^{2+}$ at the electrolyte/electrode interface, which means more energy should be applied to destroy the exterior H_2O solvation sheath, thus resulting in a low electrochemical activity. The anions in the electrolyte having no solvated effect possess higher ion mobility, which can contribute to the ionic conductivity, in return, the ion conductivity contributed by Zn^{2+} is diminished. In addition, other ions such as H^+, OH^- and SO_4^{2-} as well as the free H_2O molecules probably take part in the evolution of H_2 and generation of $Zn_4(OH)_6SO_4{\cdot}H_2O$ [67,71], which would greatly weaken the anode stability. Thus, the selective distribution of the ions at the electrolyte/electrode interface is of significance to the uniform Zn deposition. For example, Hydrogen-substituted graphdiyne (HsGDY) prepared through cross-coupling and cyclizing the 1,3,5-triethynylbenzene ($C_{12}H_6$) monomer (Large hexatomic rings in $C_{12}H_6$ has a theoretical diameter of 1.63 nm) can construct a selective ion channel with a sub-ångström level and micrographs for Zn^{2+} migration and meanwhile impair the hydrated Zn^{2+} migration(Fig. 4**g**) [37]. As mentioned above, the concentration distribution can affect the zinc growth. It is evident that the ions prefer to gather at the surface protuberance sites and the distribution concentration becomes more inhomogeneous even if the deposition only lasts for 5 s or 10 s (Fig. 4**h**). While for the zinc deposition on the HsGDY layer (Zn@Artificial interface layer), the Zn^{2+}that are about to be reduced electrochemically has to longitudinally migrate through the micro molecular tunnels, which effectively impair the direct contact of Zn^{2+} and protuberant nucleation sites. Thus, the Zn^{2+} transports homogeneously through the HsGDY layer causing uniform ion diffusion in the interconnected ion tunnels. As the simulation shows in Fig. 4**h** after deposition for 5 s or 10 s, the distributed concentration of Zn^{2+} remains uniform. The tunnel type ion transportation can be changed into a totally different hopping type ion transportation by introducing the Nafion (Containing hydrophobic and hydrophilic functional groups) into an inorganic Zn-X zeolite nanoparticles [10]. The inorganic Zn-X zeolite has a maximal nanochannel of 0.74 nm and the Nafion has a larger channel of 4 nm [72]. The organic-inorganic interface was chemically constructed via dynamically cross-linked Zn-X and sulfonate ($-SO_3^-$) groups using Zn^{2+} a bridge. In such a composite layer, the Zn^{2+} prefers to hop along with the Zn-X zeolite/Nafion interface while the H_2O and SO_4^{2-} are blocked due to the hydrophilic channels being hindered by Zn^{2+}, thus impairing the side reactions: $2H_2O + 2e^- \rightarrow H_2 + 2OH^-$ and $4Zn^{2+} + SO_4^{2-} + 6OH^- + 5H_2O \rightarrow Zn_4(OH)_6SO_4{\cdot}H_2O$.

Similar to graphene or graphite, which possess high conductivity and controllable surfaces with reactive groups, layered MXene can also function as a host material for zinc deposition. Moreover, the MXene coating on the zinc surface can effectively enhance the electrochemical stability during the zinc plating/stripping process and mitigate corrosion as well as side reactions [61]. An ultrathin and uniform MXene

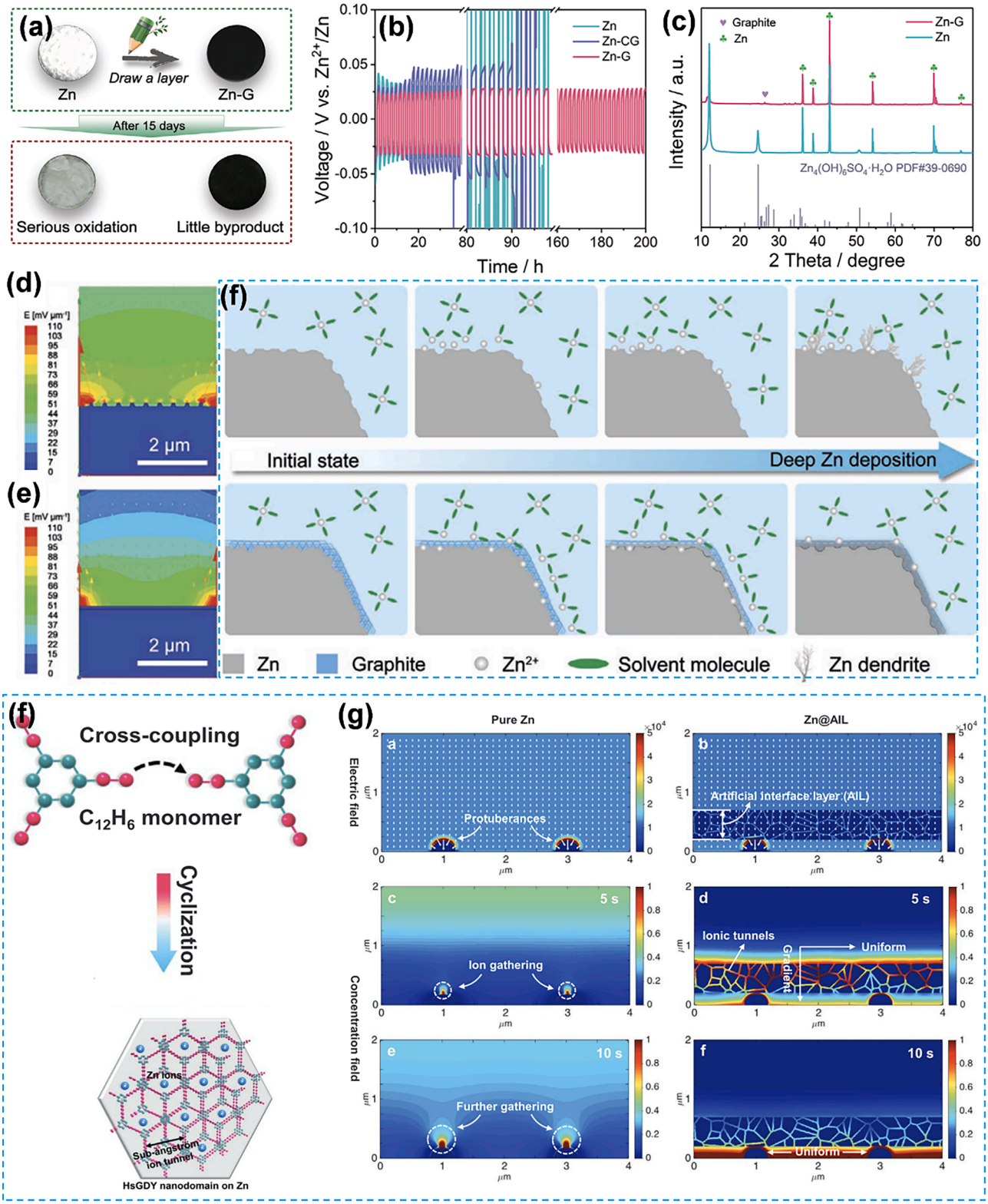

Fig. 4. (a) Digital photos of graphite-coated zinc (Zn-G) and bare zinc before and after immersing in 2 mol L^{-1} $ZnSO_4$. (b) Symmetrical cell Zn plating/stripping testing at 0.1 mA cm^{-1}. (c) XRD results of the bare zinc and graphite-coated zinc after cycling test. The electric field distributions and illustration for zinc deposition of (d) bare zinc and (e) Zn-G. (f) Illustration of zinc deposition on the surface of bare zinc and Zn-G. Reproduced from Ref. [67]. Copyright (2021) Wiley-VCH GmbH. (f) Reaction mechanism of cyclization of $C_{12}H_6$ monomer. (g) Zn^{2+} concentration distribution on the surface of pure Zn and Zn@AIL (Zn@Artificial interface layer). Reproduced from Ref. [37]. Copyright (2020) Wiley-VCH GmbH.

coating layer was fabricated on the zinc surface using an in situ spontaneous reducing/assembling approach. The electrons generated by the zinc foil are conveyed to the oxygen-containing groups on MXene flakes, which leads to the reduction of MXene flakes and a reduction in the electrostatic repulsion force among the MXene layer (Fig. 5**a**) [16]. This in situ approach can effectively prevent the weakening of integration, ensuring strong adhesion between the coating layer and substrate [73]. As shown in Fig. 5**b**, the MXene-coated zinc foil (MZn) can keep tight contact even after dramatical twisting and folding. The uniform MXene layer plays a key role in creating a homogenized electrical field, allowing control of zinc nucleation overpotential and distribution of the electrical field, which, in turn, leads to uniform zinc deposition. As depicted in Fig. 4**c**, the MZn-60 sample exhibited the lowest nucleation overpotentials at various current densities. The real-time optical monitoring in Fig. 4**d** also highlighted dendrite-free plating on the MZn-60 surface, in contrast to dendrite growth on the bare zinc surface. Simulated outcomes demonstrated a significantly more uniform distributed electrical field compared to bare zinc (Fig. 5**e-f**). It has been established that the MXene coating layer can provide a higher specific surface area for zinc deposition and enhance hydrophilicity, which facilitates ion mobility [74]. In addition, when loading MXene with zincophilic metals (For example, Sb, Cu, and Ni), the metals can act as the seed crystal for uniform zinc nucleation and growth, resulting in an enhanced stable performance [75–77]. Interestingly, MXene can also be used as an electrolyte additive. As shown in Fig. 5**g**, the oxygen-containing groups attached to the suspended MXene flakes provide numerous zincophilic sites, which contribute to the formation of a stable solid-electrolyte interface. This process ultimately leads to the primary uniform zinc deposition [78].

Although most inorganic composite coatings ensure excellent Zn plating kinetics due to their high Zn^{2+} conductivity, their inherent brittleness and weak bonding to the zinc substrate impede the high

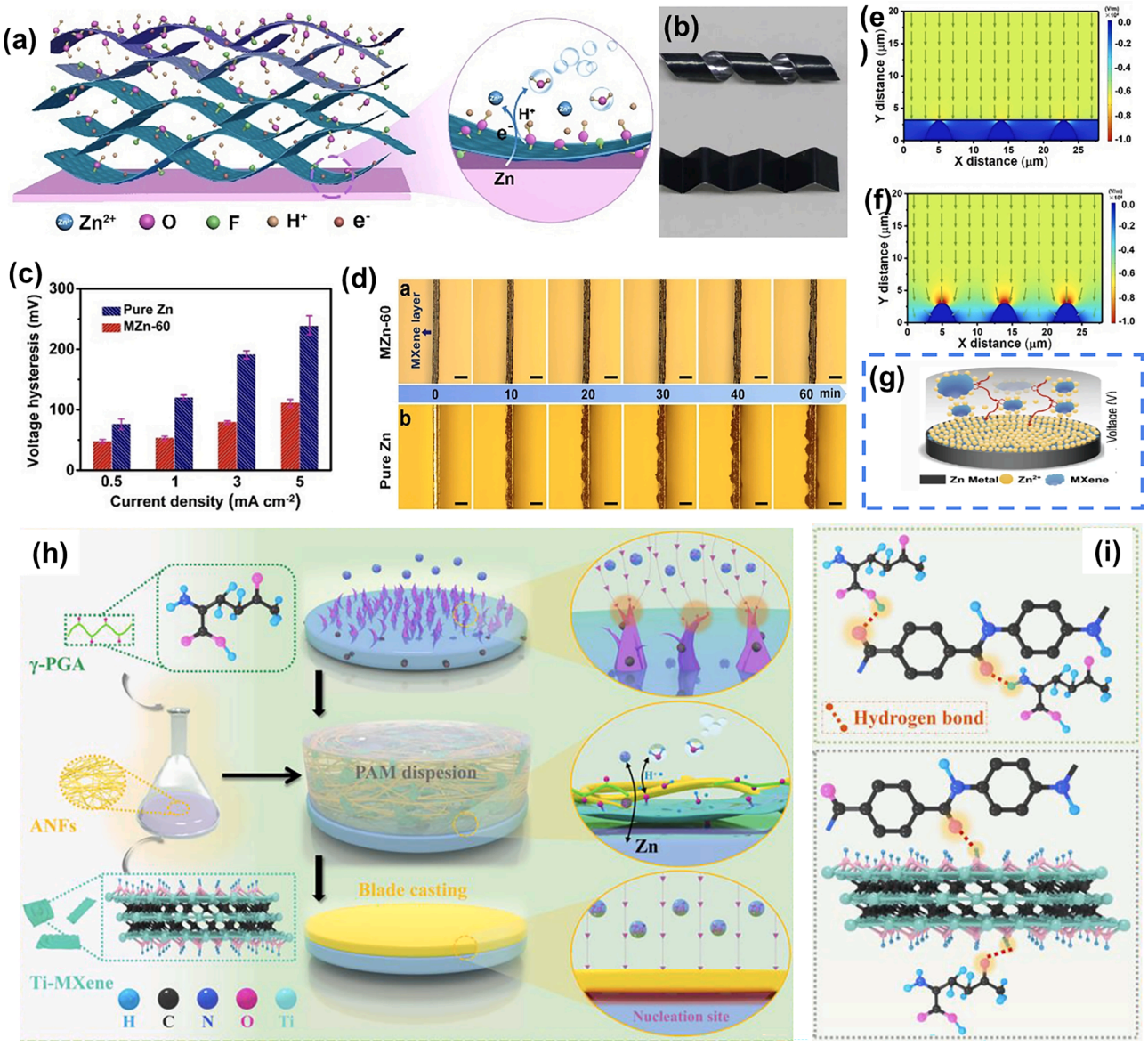

Fig. 5. (a) Illustration of the reducing and assembling process of MXene on the surface of a zinc sheet. (b) Digital photos of the MXene-coated Zn foil in twisted and bent states. (c) Voltage hysteresis of symmetrical cells at different current densities from 0.5 to 5 mA cm^{-2}. (d) In situ optical monitoring of the plating process. The simulated distributed electrical field of (e) MXene and (f) bare zinc. Reproduced from Ref. [73]. Copyright (2021) Wiley-VCH GmbH. (g) Illustration of Zn plating process in MXene-regulated electrolyte (2 M $ZnSO_4$). Reproduced from Ref. [78]. Copyright (2021) Spring Nature. (h-i) Schematic illustration of the creation of γ-poly(glutamic acid) (γ-PGA)/aramid nanofibers (ANFs)/MXene (PAM) protective coating and the formation of hydrogen bond in PAM. Reproduced from Ref. [61]. Copyright (2023) American Chemical Society.

capacity of continuous Zn deposition, which probably disables the protective layer [40]. In another study in Fig. 5**h-i** [61], organic γ-poly (glutamic acid) (γ-PGA) and aramid nanofibers (ANFs) are introduced into MXene (PAM) to prepare a composite protective coating on the zinc surface that can effectively enhance the integrity of the coating layer. The γ-PGA and Ti-MXene were first dispersed into an ANF/DMSO solution under sonication, and then the composite slurry was coated onto the zinc surface using a doctor blade. The strong hydrogen bonding between the organic molecules and the MXene substrate provides PAM with a three-dimensional (3D) network and plasticity. With this optimized PAM on the zinc surface, the corrosion resistance of the zinc anode is enhanced, and the growth of zinc dendrites is inhibited.

Although the 2D carbon/MXene-based coating layer exhibits excellent effects in enhancing the performance of a zinc anode, it should be emphasized that conductive 2D carbon/MXene materials are inherently imperfect with edges and defects that act as preferential sites for Zn^{2+} ion deposition, and possess a large specific surface area. Consequently, Zn^{2+} ions migrating from the electrolyte tend to deposit predominantly on the surface of the modified layer rather than the interior, resulting in uneven zinc deposition in the protective coating layer. Moreover, the abundant defect sites also act as active sites for hydrogen evolution, which may result in high pressure within the cell. This suggests that the conductive network of the modified layer can only homogenize the electric field and suppress dendritic growth to a certain degree. Moreover, the increased surface area in contact with the electrolyte heightens the likelihood of side reactions at the reaction interface, which continues to be a significant issue.

3.1.4. *Alloys coating layer*

An alloy is a homogeneous mixture consisting of one metal and other elements. It can be produced through processes such as smelting, powder metallurgy, sputtering, electroplating, and more. Alloys are formulated to possess properties from both of their components and are enhanced with advantageous features such as increased strength, durability, corrosion resistance, conductivity, and various other mechanical properties. For the alloys used for zinc anode coatings, the alloyed elements with less activity than zinc are required to avoid the potential competitive reaction. That is to say, the alloyed elements prefer to be Cu [12,79], Ag [11], Mn [80], Hg [81], and other inert metals. However, when zinc is alloyed with active Al [82], the Al is converted into an insulating Al_2O_3 layer that can protect zinc from corrosion, thus enabling the stability of the Zn-Al alloy electrode. Moreover, it's important to acknowledge that alloys do not represent mere straightforward physical mixtures of distinct components. In many instances, alloyed atoms are integrated into the zinc's lattice plane or supplant zinc atoms from their original positions. This process forms a solid solution with zinc, sharing the same lattice structure as zinc. Conversely, the alloyed metals can also engage in reactions with zinc to create new species, referred to as intermetallic compounds. For example, $Zn_{0.5}Ag_{0.5}$ [11], Zn_3Mn [80], Zn_5Cu [12], and Zn_3Hg [81]. Both two types of alloys can enhance corrosion resistance by adjusting the polarization potential (Fig. 6**a-b**). The polarization potential of the alloy is dependent on the metallic component. As shown in Fig. 6**c**, the theoretical calculation indicates a more inert metal induces a higher redox potential of alloys. Furthermore, in many reported works related to alloy coatings on zinc surfaces, the energy barrier of nucleation on alloy coatings was reduced [11,12]. One can see that a Zn_5Cu alloy coating layer with abundant microstructure can offer a considerable number of nucleation sites for zinc and sufficient space for zinc deposition, which endows a reduced nucleation potential of 18 mV compared to that of the bare zinc (46 mV), and keeps a stable operation over 1000 hour at the current density of 1.0 mA cm^{-2} (Fig. 6**d-f**). In the case of CuZn alloy, for example, Cu/Zn composite [79] and brass [83], it has been confirmed with positive effects on improving uniform zinc deposition and inhibiting anode corrosion. Furthermore, the phase composition and lattice structure of the CuZn alloy can be continuously adjusted throughout the zinc plating/stripping process, which can lead to various crystalline structures that might compromise the stability of the interface between the coating and electrolyte [84]. It is crucial to find out the relationship between the phase composition and deposited zinc to avoid the potential lattice mismatch or energy barrier of deposition. Impressively, a multi-component CnZn alloy including CuZn, $CuZn_5$, $CuZn_2$, and Cu_5Zn_8 coating layer was magnetron sputtered and deposited on the surface of bare zinc foil by regulating the sputtering time, which greatly multiply nucleation sites during the zinc plating due to its high binding energy to zinc atoms and limited zinc diffusion (Fig. 6**g-h**) [85]. The optimized zinc nucleation sites differ from the "tip effect" nucleation mechanism, which contributes to the reduction of zinc aggregation during the plating/stripping process. Moreover, this multi-component CuZn alloy acts as a buffer for lattice mismatch during zinc plating/stripping, while also mitigating hydrogen evolution and corrosion by creating a separation between zinc and the electrolyte through direct contact. The computed adsorption energies of CuZn alloys with various atomic ratios compared to zinc atoms are notably lower than those of pure zinc and copper substrates, as depicted in Fig. 6**h**. This signifies robust interactions and heightened zincophilicity, leading to the promotion of uniform zinc deposition. Conversely, a feeble interaction results in zinc aggregation and dendrite growth. In addition to the Zn based alloys that can be used as the protective coating layer to improve the cycling stability of anode, some inert pure metals, for example, Sn [86], Sb [87], Au [88] and Bi [89], when coated on zinc surface, are also confirmed with positive effects on improving the anodic stability.

Indeed, an appropriate alloy coating layer can mitigate the growth of zinc dendrites. However, the approaches to prepare alloy coating on zinc surface only focus on electrodeposition, chemical replacement and magnetron sputtering, which greatly limit the microstructures of the layer [1]. What's more, a profound discharge can lead to the formation of a dense layer of newly deposited zinc on the surface of the alloys, which in turn triggers hydrogen evolution and the growth of dendrites.

In contrast to solid alloys, the zinc growth on liquid metals (LM) is distinct. The electro-reduced zinc is first dissolved and diffuses into the LM, which means that the zinc does not precipitate in the LM until it achieves a saturation state (Fig. 6**i**) [90]. Therefore, the nucleation and growth of zinc on the surface of LM is greatly delayed. For the most widely used Ga-In liquid alloy, the high zinc affinity and electronic conductivity guarantee fast mass and electron transport, as well as strong adherence to the zinc substrate. Thus, the electro-reduced zinc prefers to dissolve into the Ga-In liquid alloy instead of gathering together. Even when the zinc becomes saturated in Ga-In liquid alloy, the zinc would grow inward rather than upward on the liquid alloy/electrolyte interface [91–93]. Such the temporally and spatially asynchronous zinc electro-reduction and growth endows simultaneously fast Zn redox kinetics and dendrite-free Zn (002) deposition [94], which can effectively eliminate the dendritic growth. It should be pointed out that the liquid Ga-In layer is electrochemically inert because the maximum solubility of zinc in Ga-In liquid alloy is only 3.22 wt% at room temperature (25°C). This only contributes an extremely low capacity of 14 mAh g^{-1} compared to the zinc anode (820 mAh g^{-1}) [90,95,96]. Furthermore, the corrosion resistance can be also enhanced by increasing the overpotential of the HER [90]. Based on the analysis above, the Ga-In liquid alloy is a chemically stable and valuable buffer layer for zinc plating/stripping. As shown in Fig. 6**j**, Galinstan liquid metal (LM) was brushed on a silver-coated Nylon textile (AgT) conductive base to construct the LM-AgT anode. The LM after being loaded with zinc can function as an anode for ZIBs. One can see that the XRD patterns for the zinc deposition on LM-AgT anode and bare AgT anode with different zinc deposition capacities display obvious differences. The ratios of I_{002}/I_{101} LM-AgT are much higher than that of the bare AgT (about 0.45 with different zinc deposition capacities), indicating the growth direction of zinc prefers to be Zn(002) on the LM-AgT anode. Furthermore, to evaluate the effects of LM on zinc deposition, an asymmetrical cell was assembled, and 5 mAh cm^{-2} Zn deposition was

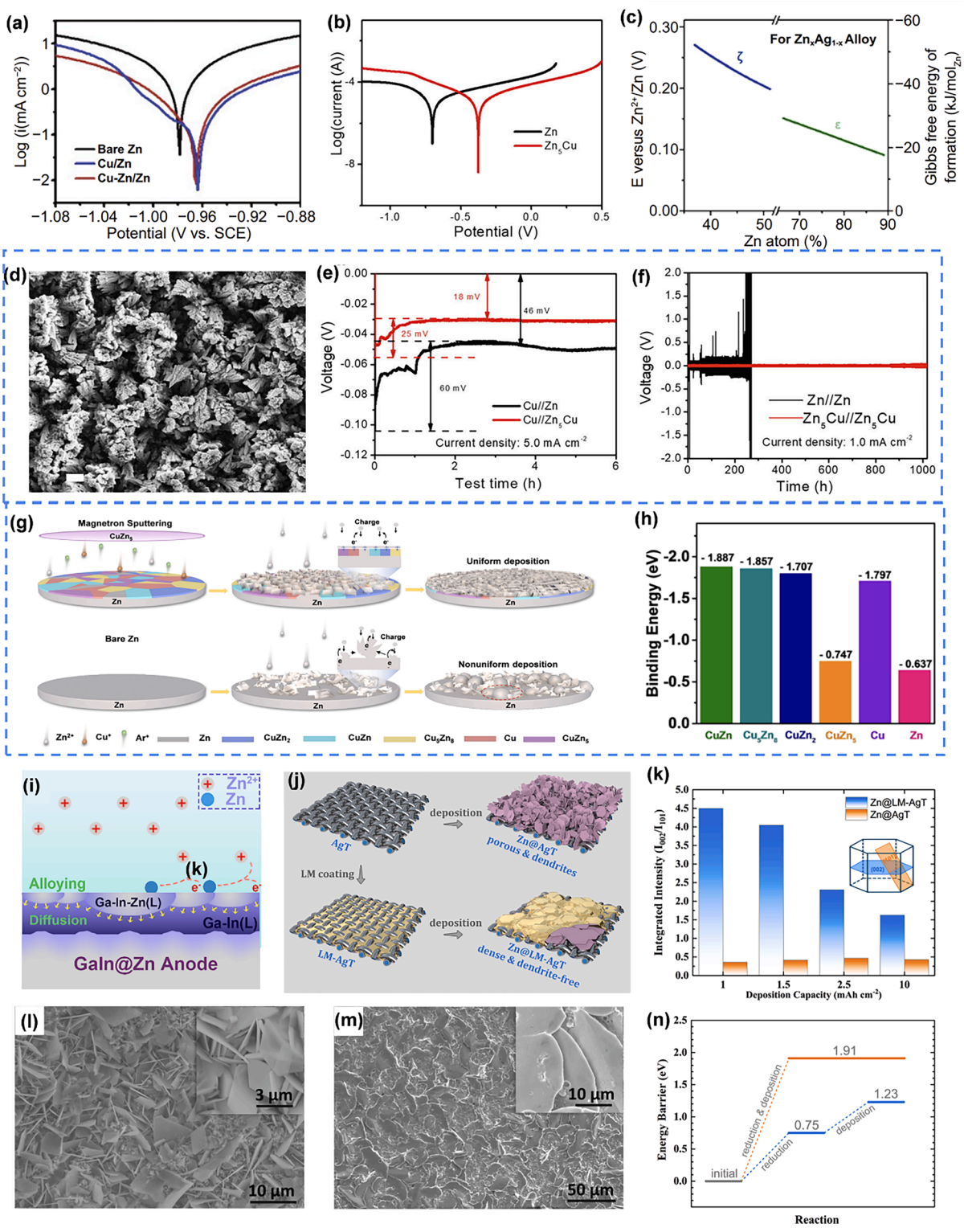

Fig. 6. (a) Linear polarization curves of Cu/Zn and Cu-Zn/Zn electrodes in 3 M $ZnSO_4$. Reproduced from Ref. [79]. Copyright (2020) Elsevier. (b) Linear polarization curve of Zn_5Cu electrode in 2 M $ZnSO_4$. Reproduced from Ref. [12]. Copyright (2022) Springer Nature. (c) Theoretical Gibbs free energy of formation and electrochemical potential shift versus Zn^{2+}/Zn for ε-Zn_xAg_{1-x} alloy. Reproduced from Ref. [11]. Copyright (2021) American Chemical Society. (d) SEM images of electro-deposited Zn_5Cu on zinc foil. (e) Nucleation potential of Zn_5Cu at the current density of 5 mA cm^{-2} and (f) corresponding symmetrical cell testing at the current density of 1 mA cm^{-2}. Reproduced from Ref. [12]. Copyright (2022) Springer Nature. (g) Preparation process of Cu-Zn@Zn electrode and uniform zinc deposition, and non-uniform zinc deposition on bare zinc. (h) Adsorption energy of Zn atoms absorbed on CnZn, Cu_5Zn_8, $CuZn_2$ and CuZn. Reproduced from Ref. [85]. Copyright (2022) Wiley-VCH GmbH. (i) Schematic illustration of dendrite-free GaIn@Zn anode with an alloying−diffusion synergistic mechanism. Reproduced from Ref. [90]. Copyright (2021) American Chemical Society. (j) The design of the LM-AgT anode. (k) Values of XRD intensity ratio of $I_{Zn(002)}/I_{Zn(101)}$ of Zn@AgT and Zn@LM-AgT anodes with different Zn deposition capacities (mAh cm^{-2}). SEM images of zinc deposited on (l) Cu and (m) LM@Cu after 5 mAh cm^{-2} Zn deposition. (n) Calculated energy barriers for the Zn deposition process on Cu substrate (orange) and LM (blue). Reproduced from Ref. [94]. Copyright (2023) Elsevier.

applied (Fig. 6**k**). A random orientation and horizontal orientation of hexagonal Zn flakes were found to grow on the bare copper surface and LM-coated copper surface, respectively, which confirmed a planar growth with exposed (002) facets of zinc on the LM surface (Fig. 6**l-m**). The DFT calculation of the energy barriers for Zn migration through electrolyte/electrode interfaces indicated that the energy barrier for Zn^{2+} to Zn_L (dissolved in the LM) and Zn_C (crystalized zinc) are 0.75 eV and 1.23 eV, respectively, which were much lower than that of the bare copper (1.95 eV, Fig. 6**n**). This means the electro-reduced zinc prefers to dissolve in the LM rather than directly depositing on the LM surface, resulting in delayed zinc nucleation. In addition, the lower surface energy of Zn(002) on the LM surface of 14.37 J m^{-2} compared to that of the Zn(101) (17.21 J m^{-2}) also endows the preferential growth of Zn (002) underneath the LM interface. Attributed to those advantages of the LM coating layer, the LM-AgT anode displays an enhanced long-term cycling performance over 700 h. Interestingly, a quarternary solid-liquid composite (SLC) of Ga-In-Sn-Zn was developed for rechargeable ZIBs. The results show that solid phase $InSn_4$ in SLC reduces the diffusion energy barrier of zinc ions due to the strong affinity to zinc atoms. The inert Ga-In LM eases the stress variation during the plating/stripping process, thus resulting in a uniform zinc deposition [97].

Various strategies are employed in constructing protective coating layers on zinc surfaces. To elucidate the diversities and similarities among these strategies, a comparison diagram based on the mainly reviewed works is presented in Fig. 7. The most commonly used strategies for preparing protective coating layers on zinc surfaces, as indicated in Fig. 7, include (Electro-)Chemical reactions and casting. Notably, regarding of the inorganic metal/nonmetal compounds based protective coating layer, the layer can be in situ constructed on the zinc surface by simple chemical reaction, or directly coating the oxides onto the zinc surface with a doctor blade or drop coating (here named as casting). For example, the directly bonding of 2-methylimidazole (2-MeIm) with ZnO layer on Zn surface and UV radiation of the photosensitive polydopamine can construct organics on the zinc surface, which ensure a strong adhesion of the organics on zinc surface. Another effective strategy is casting, directly coating the organics on the zinc surface. Concerning the 2D carbon/MXene-based coating layer, it should be pointed out that not only the casting strategy can be used, the physical adsorption is also widely used to prepare a protective coating layer due to the strong electrostatic repulsion interaction between the coatings and zinc surface. In contrast to the above-mentioned coating layers, the alloy protective coating layer shows unique characteristics. In general, metals can be electrochemically reduced at a chosen potential, thereby creating an alloy layer on zinc surface. However, induction melting and liquid anode strategies are distinctive in the preparation of alloy coatings. In addition to the solid alloy coating layers prepared by other strategies, the liquid anode approach is distinct and heavily relies on the most commonly used Ga-In liquid alloy. This ensures a liquid state of an alloy layer. The high zinc affinity and electronic conductivity of liquid alloy not only guarantee strong adherence to the zinc surface but also ensure fast mass and electron transport, which further induces the inward growth in the liquid alloy of the electric-reduced zinc. The various approaches highlighted in this summary provide valuable insights into the preparation of effective protective coating layers.

3.2. The design of host materials for ZIBs anode

Direct modification on zinc sheets has been widely explored and made great achievements. However, there remain some problems. For example, the process of zinc plating/stripping would introduce huge volume changes, damaging the protective coating layer. Particularly, this phenomenon becomes pronounced under highly demanding charge-discharge conditions. Additionally, the surplus quantity of employed zinc sheets far exceeds the requisite zinc source during the discharge process, resulting in a low depth of discharge (DOD). Hence, the creation of a composite anode possessing high plasticity and reduced zinc content holds paramount significance. Fulfilling this requirement can be achieved by directly fabricating a coating layer on non-zinc substrate. The main objectives remain centered around achieving dendrite-free zinc growth and reducing the occurrence of the HER. Delaying the time when the dendrites start to grow can effectively enhance the anode stability, which can be achieved by reducing the effective electrode current density (EECD) [14]. That is to say, creating a three-dimensional architecture for an anode with an increased specific surface area proves beneficial. This designed approach can lower the EECD and overpotential by facilitating ample charge/mass transfer and offering numerous zinc nucleation sites [1]. In addition, creating zincophilic and inert HER sites in the host materials are also significant, as it can induce uniform zinc deposition and suppress hydrogen generation,

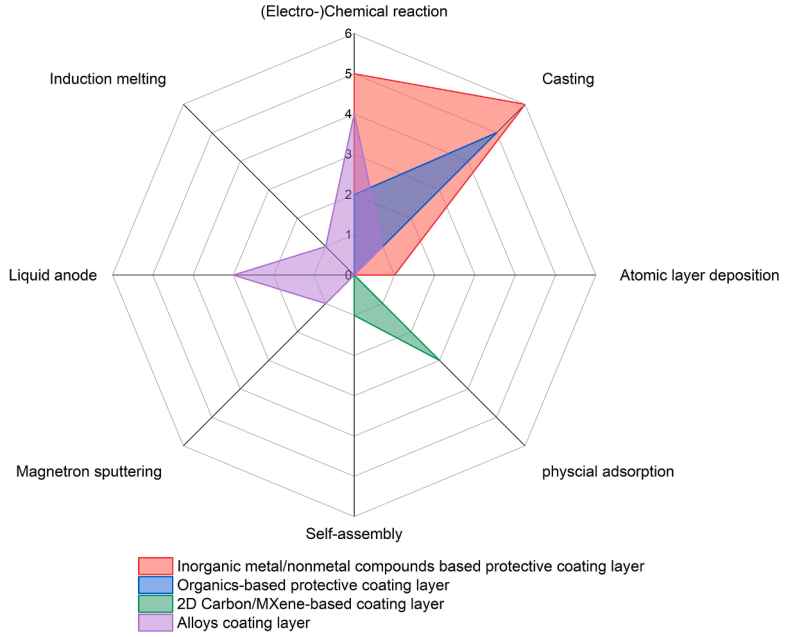

Fig. 7. A comparison diagram of various protective coating strategies.

respectively. Some reported host materials for ZIBs anode can be found in **Table S2**.

A carbonaceous framework with excellent conductivity and lightweight characteristics, as well as a good zincophilic property for zinc deposition, is promising as a zinc host in many works. For example, the 3D MOF-derived carbons. It should be emphasized that the carbonaceous substrate can not be directly used as the anode for ZIBs because the zinc source in anodes is essential during the stripping process. Therefore, the zinc source should be loaded in the substrate in advance, forming a zinc/carbon composite electrode. For example, the

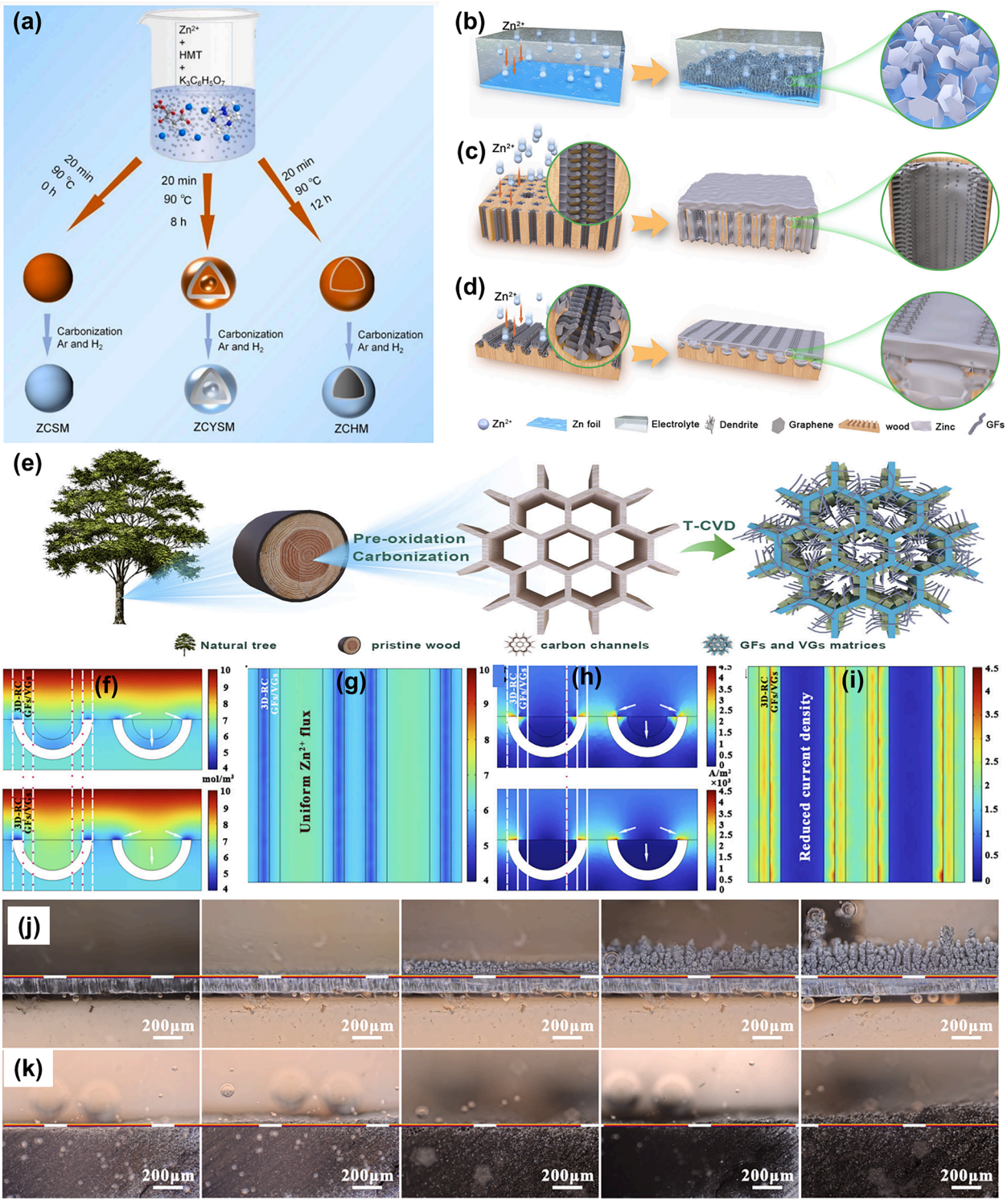

Fig. 8. (a) Illustration of the preparation of yolk-shell microspheres (ZCYSM) as zinc host materials. Reproduced from Ref. [98]. Copyright (2023) Wiley-VCH GmbH. Illustration of 3D ordered microstructure containing vertical graphene arrays (VAs) and graphene nanofibers cluster (GFs): Zn deposition on a bare (b) Zn, (c) 3D-LFGC, and (d) 3D-RFGC. (e) Process of preparing 3D-LFGC and 3D-RFGC zinc host materials. (f) Simulated Zn^{2+} concentration distribution and (g) corresponding top-view image for 3D-RFGC@Zn. (h) Simulated current density distribution and (i) corresponding top-view image for 3D-RFGC@Zn. Optical interface evolution of zinc deposition on (j) a bare Zn anode and (k) 3D-RFGC@Zn anode at a current density of 40 mA cm^{-2}. Reproduced from Ref. [100]. Copyright (2023) Springer Nature.

ZCYSM@Zn (yolk-shell microspheres@Zn) electrode is fabricated by pre-galvanizing zinc on the ZYSM coating layer, ensuring the necessary zinc source during the plating/stripping process (Fig. 8**a**) [98]. The prepared ZCYSM@Zn electrode can regulate the Zn^{2+} flux and keep excellent cycling stability due to the superior buffering effect. The zinc deposition takes place in the interior of ZYSM, effectively restraining the expansion of zinc deposition during the cycling process [98]. Similarly, carbon nanotubes have also been confirmed as an optimized conductive framework to prepare a dendrite-free anode for ZIBs by homogenizing the distributed electrical field [99]. In many works, the ion concentration and distributed electrical field are more homogeneous compared to that of bare zinc. However, the structural orientations of the host materials are sequential. Recently, the difference in zinc deposition behaviors on biomass wood-derived vertical and radial direction of carbon channels have been explored **(**Fig. 8**b-e)** [100]. At first, the carbon channels including the longitudinal direction carbon (3D-LC) and radial (3D-RC) direction carbon are prepared by pre-oxidation and carbonization process. The ordered structure comes from the nature of the biomass wood. To obtain abundant surface structure, vertical graphene arrays (VAs) and graphene nanofibers clusters (GFs) are grown on the channels of 3D-LC and 3D-RC using CH_4 as the carbon source. Finally, to construct a 3D zinc anode, zinc is directly deposited on the 3D carbon frameworks (3D-LFGC and 3D-LFGC matrices). As we all know, the zinc deposition on bare zinc surfaces tends to form dendrites. While on the surface of the 3D-LFGC and 3D-RFGC matrices, the 3D structure with full of ordered multichannel and surface pores can provide abundant space for zinc deposition. In addition, the zincophility properties of the carbon substrates can induce dense zinc deposition. Because the 3D-RFGC has larger open area than that of the 3D-LFGC, 3D-RFGC can provide shorter Zn^{2+} diffusion pathway and more nucleation sites than that of the 3D-LFGC. The simulated results in Fig. 8**f-g** indicate the Zn^{2+} concentration on the different positions (3D-RC and GFs/VGs) of the 3D-RFGC framework are different. One can clearly find that the ion concentration close to the internal and external channels of the 3D-RFGC frameworks displays more uniform and is lower than that of the 3D-RC, implying the uniform zinc deposition on the inner wall. While for the 3D-RC without GFs and VGs decoration, the zinc prefers to grow on the top sites rather than the inner wall. Furthermore, the distributed current density on the surface of the 3D-RFGC also displays a similar distribution as Zn^{2+} ion concentration. As shown in Fig. 8**h-i**, higher local current density is gathered on the top of 3D-RC, but much more uniform on the internal and external channels, further indicating the introduced GFs and VGs can optimize the zinc growth. The in situ optical interface evolution indicated the small Zn particle appeared on the bare zinc surface after deposition for 10 min and the obvious zinc dendrites were formed as the continuous zinc deposition. However, a dendrite-free zinc deposition and smooth surface were achieved on the 3D-RFGC@Zn anode surface (Fig. 8**j-k**).

Of course, the carbon materials can be coupled with metals (named as metal/carbon) as the zinc host materials, for example, the AgNPs@CC electrode constructed with Ag nanoparticles and commercial carbon cloth was also developed with excellent zinc deposition interface via forming zincophilic $AgZn_3$ alloy [101]. Zincophilic atomically dispersed metal atoms (For example, Cu and Zn sites) on N, P-codoped 3D carbon framework can maximize the active zinc nucleation sites, resulting in a low Zn nucleation overpotential and dendrite-free Zn deposition [102]. In addition, because of the existence of metal particles in metal/carbon host materials, the lattice structure difference between metal and zinc also has great effects on the nucleation and growth of zinc. The different lattice structure between zinc and substrate would result in the formation of an incoherent interface, inducing defects and charge accumulation. However, a similar lattice structure with a small lattice mismatch between the zinc and substrate prefers the formation of semi-coherent and coherent interfaces, which is beneficial to weaken the energy barrier of zinc nucleation and promote the growth of zinc in a planar pattern. For example, cobalt metal in a metal/carbon host has a small lattice mismatch of 6.1 % to pure zinc, which tends to induce 3D diffusion on Zn (002), forming regular Zn alignments and suppressing dendrite formation [103].

As discussed above, the lattice mismatch between zinc and host materials has unpredictable effects on zinc growth. Furthermore, the metal-based substrate is rigid, the lattice parameter of which is hard to change and match the deposited zinc. Therefore, it probably causes an inevitable lattice deformation in the deposited zinc layer. Thus, introducing a soft layer to buffer lattice deformation can effectively improve the quantity of deposited zinc. By simply coating layered graphene on the surface of stainless steel using a specially designed doctor-blade–type apparatus, a preferential orientation for zinc parallel rather than vertical epitaxial growth was achieved, which avoids the potential dendrites (Fig. 9**a-c**) [24]. It can be found that zinc vertically grows on the surface of stainless steel and displays a closest packed plane of $[0002]_{Zn}$. For the case of graphene-coated stainless steel, the deposition of zinc on graphene coating is well directed, demonstrating a fixed parallel orientation relationship with the graphene coating layer dendrites (Fig. 9**d**). Such favorable growth direction of zinc is attributed to the low lattice mismatch of 7 % (Fig. 9**e**) between zinc and graphene because low lattice mismatch can greatly reduce the residual stresses and impose minimal lattice strain. The coulombic efficiency of graphene-coated stainless steel (GSS) electrode stabilized at about 99.7 % (after 2000 cycles) even under an ultra-high current density of 40 mA cm^{-2} and an area capacity of 3.2 mAh cm^{-2} (Fig. 9**f**). In addition, the full cell of MnO_2||GSS also displays much better stability than that of the stainless steel and bare zinc foil (Fig. 9**g**). In addition to the lattice parameter between the substrate and zinc epi-layer affecting the zinc deposition, the surface defects of graphene layers are also crucial to the zinc plating process through introducing favorable defects for nucleation and homogenizing the surface distributed electric field [67].

In addition to regulating the lattice parameter between the deposited zinc and substrates, lots of substrates with initial structural stability and affinity to zinc, for example, the 3D porous metal framework (porous copper, porous nickel, copper mesh) [104–107], was used for assembling a long-life anode. A 3D porous substrate has a larger specific surface area than that of a plane substrate, which can ensure more zinc nucleation sites and enough space for zinc growth in a restricted scope, thus achieving dendrite-free zinc growth.

Based on the foregoing analysis, it is evident that the majority of host materials for ZIBs anodes possess a porous structure with 3D architecture. This necessitates higher costs in designing effective materials, due to the complexity of the manufacturing processes. Moreover, the introduction of zinc into these host materials prior to their utilization as anodes complicates the anode preparation procedures.

3.3. Intercalated anode

As summarized above, a considerable amount of work has been focused on zinc modifications or designing zinc hosts to mitigate dendrite growth and side reactions. However, the huge volume change during the zinc plating/stripping process can't be ignored. Seriously, some zinc dendrites may fall off from the current collects before puncturing the separators and become "dead zinc", which reduces the utilization ratio. In addition, for the composite anodes whatever with or without zinc substrate would increase the mass of the anode, resulting in a reduced gravimetric specific capacity of full cell ZIBs. One of the most promising strategies to overcome those disadvantages is developing intercalated anodes for ZIBs, which avoids the direct use of metallic zinc [9]. In other words, it is a type of material that stores or releases energy via the intercalation/deintercalation of Zn^{2+}. Because of the absence of zinc metal, the dendrite growth of zinc and corrosion are completely excluded. Furthermore, the intrinsic storage capacity of an intercalated anode can maximize the utilization rate of raw materials instead of solely being used as a substrate for zinc deposition.

A proper intercalated anode for ZIBs requires excellent conductivity,

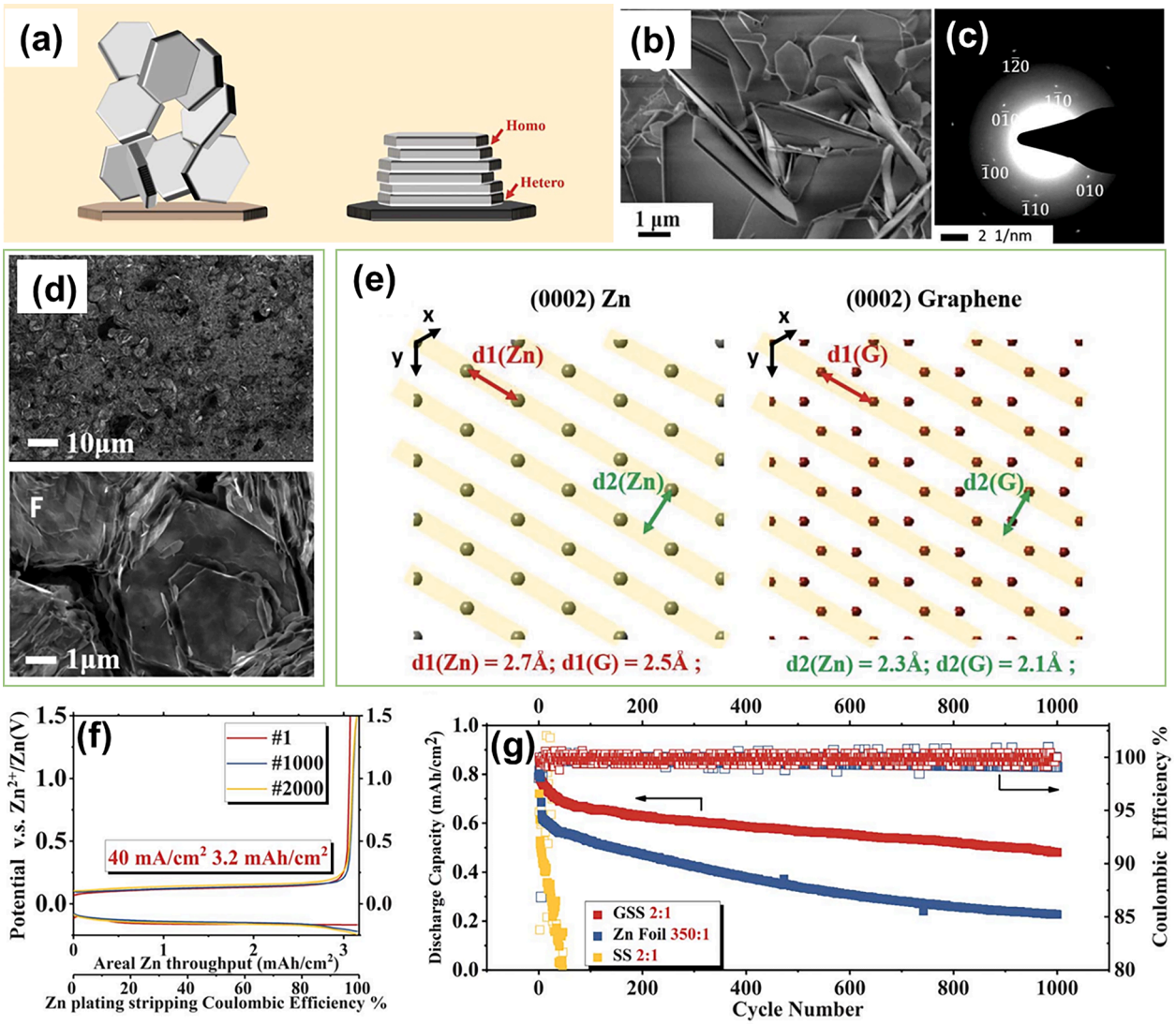

Fig. 9. (a) Illustration of vertical and parallel growth of zinc. Scanning electron microscopy (SEM) images of Zn growth on (b) bare stainless steel and (d) graphene-coated stainless steel under a current density of 4 mA/cm^2. (c) TEM diffraction pattern of Zn on bare stainless steel. (e) Atomic lattice structure of $(0002)_{Zn}$ and $(0002)_{Graphene}$. (f) Columbic efficiency of Zn||GSS. (g) Cycling performance of GSS, zinc foil, and SS paired with MnO_2. Reproduced from Ref. [24]. Copyright (2022) American Association for the Advancement of Science.

large Zn^{2+} storage capacity, and low potential vs. zinc (low Zn^{2+} insertion potential) [9,108]. However, few works about the intercalated anode for ZIBs are reported, and a definitive Zn^{2+} storage mechanism remains unclear, which presents a great challenge to the development of intercalated anodes with high capacity and high energy density. Until now, the intercalated anodes can be classified into the following:

(1) Inorganic materials. Inorganic intercalation anode materials should possess reversible interlayer spaces or lattice tunnels available for the insertion/extraction of Zn^{2+}. During the discharge stage, Zn^{2+} inserts into the crystal unit of an intercalation anode material, gradually triggering a phase change. Taking the Mo_6S_8 intercalation anode material as an example, as demonstrated in the following two reactions [18], Zn^{2+} gradually inserts into Mo_6S_8 to form $ZnMo_6S_8$ and ultimately forms $Zn_2Mo_6S_8$ during the discharge process. In the charge process, the Zn^{2+} is released from $Zn_2Mo_6S_8$. As the energy storage/release relies on the insertion/extraction of Zn^{2+}, an advanced intercalated anode material that facilitates rapid and reversible Zn^{2+} transportation is crucial.

$$Zn^{2+} + Mo_6S_8 + 2e \rightarrow ZnMo_6S_8$$

$$Zn^{2+} + ZnMo_6S_8 + 2e \rightarrow Zn_2Mo_6S_8$$

Currently, the chalcogenide-based inorganic materials contributed to most studies for inorganic compound materials for the intercalated anode of ZIBs, including monoclinic MoOx [109], hexagonal MoO_3 [110], WO_3/3D porous graphene [111], CuS_{1-x} [112], CuS@CTMAB [113], MoS_2 [114], Chevrel phase Mo_6S_8 [18,19], TiS_2 and $TiSe_2$ [115, 116], $ZnMo_6S_8$ and $Zn_2Mo_6S_8$ [117], $MoTe_{1.7}$ [118], $TiTe_2$ [119], $Na_{1.6}TiS_2/CuSe_2$ [120]; On the other hand, many complex compound, for example, $Ti_2O(PO_4)_2{\cdot}2H_2O$ [121], $BiOIO_3@Zn_3(PO_4)_2{\cdot}4H_2O$ [122], BiOX (X = Cl, Br, I) [123,124], Sn-doped BiOCl [125], Ni-doped $Bi_2O_2CO_3$ [126] are also explored (**Table S3**), which were designed with a principle of introducing groups or atoms with large size to the layer materials to extend the layer spacing of the host materials.

(1) Organic materials. Organic materials constitute another crucial category of cation-storage materials facilitated by redox-active groups (e.g., quinone O, pyrazine N, hexaazatrinaphthalene N)

[127–129]. Cation storage in these organic materials occurs through the reduction of redox-active groups, resulting in the formation of radical anions and their coordination with cations. Importantly, this process incurs negligible structural damage to the organic materials. Accordingly, the potential for high-performance Zn^{2+}-storage electrodes lies in the creation of polymers that exhibit structural stability, possess abundant redox-active centers, and feature precisely defined ion diffusion channels. Recently, some organics have been reported as effective intercalation anode materials for Zn-ions batteries. For example, poly 3,4,9,10-perylentetracarboxylicdiimide, PPTCDI [20]; perylene-3,4,9, 10-tetracarboxylic diimide, PTCDI [29]; 3, 4, 9,

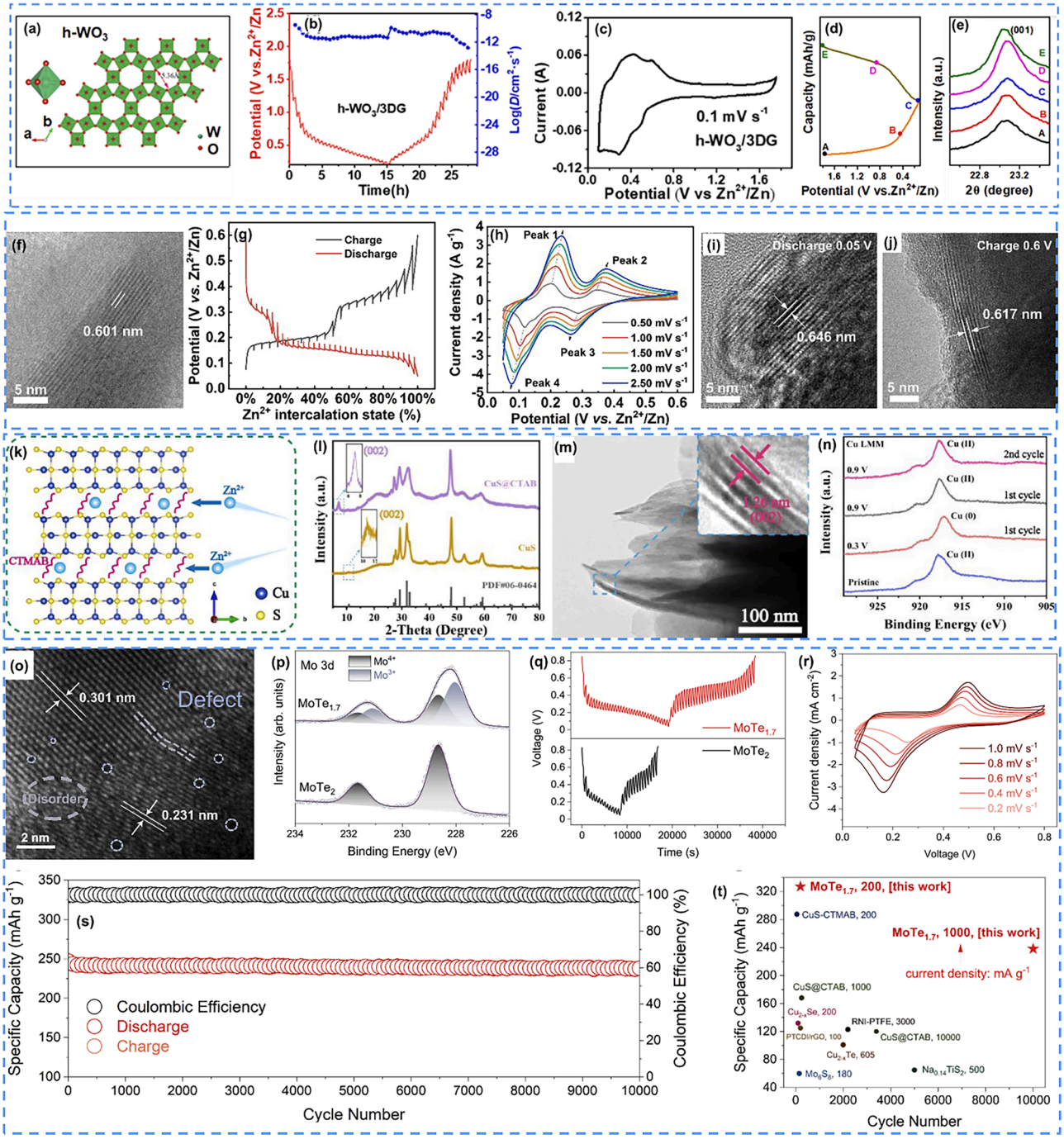

Fig. 10. (a) Crystallographic structure of h-WO_3. (b) GITT curves and diffusion coefficients, (c) CV curve, and (d-e) charge/discharge curves and corresponding ex-situ XRD patterns of h-WO_3/3DG//Zn battery in 3.0 M $Zn(CF_3SO_3)_2$ aqueous electrolyte. Reprinted with permission from Ref. [111]. Copyright (2023) American Chemical Society. (f) TEM images and (g) GITT curves of $TiSe_2$. (h) CV curves of $TiSe_2$ in 2.0 M $ZnSO_4$. High-resolution TEM (HR-TEM) images of $TiSe_2$ corresponding to the fully (i) discharged and (j) charged states. Reprinted with permission from Ref. [116]. Copyright (2022) Elsevier. (k) Illustration for CuS@CTMAB and its Zn^{2+} intercalation process. (l) XRD pattern of CuS and CuS@CTMAB. (m) High resolution-TEM images of CuS@CTMAB. (n) Auger Cu LMM spectra of the CuS@CTMAB electrodes in the pristine and fully discharge/charge states. Reprinted with permission from Ref. [113]. Copyright (2022) American Chemical Society. (o) The HR-TEM image of $MoTe_{1.7}$. (p) XPS Mo 3d spectra for $MoTe_2$ and $MoTe_{1.7}$. (q) GITT profiles and (r) CV curves at different scanning rates, (s) cycling stability at 1 A g^{-1} in 3 M $Zn(CF_3SO_3)_2$ aqueous electrolyte of $MoTe_{1.7}$. (t) Performance comparison of $MoTe_{1.7}$ with other materials for ZIBs. Reprinted with permission from Ref. [118]. Copyright (2022) Elsevier.

10-perylenetracarboxylic dianhydride, PTCDA [130]; poly-arylimide covalent organic framework (PI-COF) [108]; 1,4,5, 8-naphthalenetetracarboxylic dianhydride, NTCDA [131] (**Table S3**). To further improve the capacity of the intercalated anode of ZIBs, it is necessary to undertake the basic Zn^{2+} storage mechanism of different types of materials.

Based on the analysis presented in this section, the design principles for intercalation anode materials in ZIBs (Zinc-Ion Batteries) can be summarized as follows:

(1) High electrical conductivity, ample Zn^{2+} storage capacity, and a low potential relative to zinc.
(2) Inorganic intercalation anode materials ought to exhibit reversible interlayer spaces or lattice tunnels that accommodate the insertion and extraction of Zn^{2+}.
(3) Organic intercalation materials should contain redox-active groups capable of forming radical anions and their coordination with cations.

3.3.1. *Inorganic materials*

The intercalated anode of ZIBs functions through the insertion/extraction of Zn^{2+}, thus the ion channels in the materials significantly affect the behavior of the performance. Generally, chalcogenide-based materials with oxides, sulfides, selenides, tellurides, or their composites as active materials exist in a crystalline state and have different lattice spacing due to their different basic characteristics. A suitable pore channel or facet spacing that can be used for Zn^{2+} transportation is the key point for designing an effective intercalated anode material. To build enough space for Zn^{2+} migration, the atomic radius prefers to be larger. For chalcogenides, transition metals are always used to prepare intercalated anodes. As shown in Fig. 10**a**, hexagonal WO_3 with a channel diameter of 5.36 Å (Corresponding to the (001) plane of h-WO_3) was developed for intercalated anodes of ZIBs [111]. Its larger channel diameter than that of the Zn^{2+} (0.73 Å) provides the available migration route for the insertion/extraction of Zn^{2+}. Furthermore, the composite of h-WO_3/3D graphene (h-WO_3/3DG) has a higher specific surface area compared to h-WO_3, which further offers ion-accessible channels, enhanced conductivity and diffusion coefficient of Zn^{2+} ($D_{Zn}^{2+} = 10^{-9.5}$ to $10^{-12.8}$ $cm^2\ s^{-1}$) (Fig. 10**b**). The h-WO_3/3DG exhibits a low potential of insertion/extraction below 0.6 V vs. Zn^{2+}/Zn (Fig. 10**c**), demonstrating the potential ability to be an anode for ZIBs. The ex-situ XRD patterns of h-WO_3/3DG with different charge/discharge state displays the peak shift (Fig. 10**d-e**). The right and left shift of (001) diffraction during the discharge and charge process demonstrate the Zn^{2+} intercalation and extraction, respectively, which imply the structural reversibility of h-WO_3/3DG. Sulfur (S), selenium (Se), and tellurium (Te) have larger atomic radius than that of oxygen (O). When they are used to construct compounds, the facet spacing of the compounds may be enlarged, which is beneficial for the Zn^{2+} intercalation and extraction and further improves the performance of intercalated anodes. For example, few-layered $TiSe_2$ can be prepared by ultrasonic peeling of bulk $TiSe_2$ due to its low van der Waals forces between the interlayers [116]. The intrinsic facet spacing along the [001] direction is 6.01 Å (Fig. 10**f**). The D_{Zn}^{2+} of $TiSe_2$ is in the range of 10^{-9} to 10^{-10} $cm^2\ s^{-1}$, which is higher than that of the h-WO_3/3DG ($D_{Zn}^{2+} = 10^{-9.5}$ to $10^{-12.8}$ $cm^2\ s^{-1}$, see above), indicating the larger facet spacing can facilitate the Zn^{2+} diffusion (Fig. 10**g**). The $TiSe_2$ exhibits an extremely low discharge potential approaching 0 V vs. Zn^{2+}/Zn (Fig. 10**h**), further implying the competitive candidate to replace pure zinc as the anode. The fully discharged and charged $TiSe_2$ exhibits an increasing facet spacing of 0.646 nm and 0.617 nm, respectively, indicating the Zn^{2+} insertion/extraction in the facet lattice of $TiSe_2$ (Fig. 10**i-j**). Furthermore, the intrinsic spacing of the facet can be extended via pre-intercalation of heterogeneous molecules [113] and atoms [115]. For example, cetyltrimethylammonium bromide (CTMAB) was used to enlarge the layer spacing of CuS, as shown in Fig. 10**k**. After the pre-intercalation of CTMAB into CuS (CuS@CTMAB), the XRD peak of (002) facet shifts from 10.81°(CuS) to 6.92°(CuS@CTMAB), demonstrating an enlarged facet spacing of 1.26 nm (Fig. 10**l-m**). The as-prepared CuS@CTMAB anode has a D_{Zn}^{2+} of 10^{-10} to 10^{-12} $cm^2\ s^{-1}$, and a suitable insertion potential of~0.37 V (vs Zn^{2+}/Zn). Impressively, the reversible capacity of CuS@CTMAB has an excellent specific capacity of 350.3 mAh g^{-1} (0.2 A g^{-1}) which is much higher than the discussed h-WO_3/3DG (115.6 mAh g^{-1} at 0.1 A g^{-1}) and $TiSe_2$ (128 mAh g^{-1} at 0.2 A g^{-1}). Interestingly, this highly enhanced specific capacity results from both the Zn^{2+} insertion into the layer spacing and the conversion reactions, which is a two-step process. The Zn^{2+} first inserts into the layer of CuS to generate a new phase of ZnxCuS ($CuS + xZn^{2+} + 2xe^- \leftrightarrow Zn_xCuS$) which will lead to a lattice expansion, and then ZnxCuS concerts into ZnS and Cu (Zn_xCuS + (1-x) Zn^{2+} + 2(1-x)e^- ↔ ZnS + Cu, energy barrier of this conversion reaction is greatly reduced by introducing CTMAB). The XPS spectrum of the original CuS@CTMAB is positioned at 917.8 eV, which is attributed to CuS. Upon discharge to 0.3 V, the binding energy undergoes a downward shift to 917.0 eV, indicating a reduction involving Cu^{2+} and Cu^0. Additionally, the peak restores to 917.7 eV upon reaching fully charged states, demonstrating the reversible electrochemical reduction of the Cu^{2+}/Cu^0 pairing (Fig. 10**n**).

Another effective strategy to construct Zn^{2+} channels is to create defects in the active crystals. Tellurium (Te), among the non-metallic chalcogens, has the largest atomic radius, which has been used as the intercalated anode in some works. For example, the $MoTe_{2-x}$ with tellurium vacancies (TVs) can be used for Zn^{2+} storage. The theoretical calculation first confirms that the TVs in $MoTe_{2-x}$ can facilitate solid-state diffusion of Zn^{2+} and enhance electrical conductivity [118]. Furthermore, the lower difference of tellurium in electronegativity with molybdenum compared to other chalcogens (O, S, and Se) endows a lower redox potential [132]. $MoTe_{1.7}$ with TVs prepared by the treatment of KrF laser displays the disordered lattice structure and the TVs of $MoTe_{1.7}$ (lattice plane distance = 0.231 nm) (Fig. 10**o**). The XPS of $MoTe_{1.7}$ indicates the introduction of defects (TVs) results in a partial transformation of Mo^{4+} to Mo^{3+}, which displays an enhanced electrical conductivity of MoTe1.7 (0.31 S m^{-1}) compared to the $MoTe_2$ (0.05 S m^{-1}) (Fig. 10**p**). Because of those advantages of $MoTe_{1.7}$, higher $D_{Zn}^{2+}$of $MoTe_{1.7}$ and low insertion potential of 0.2 V vs. Zn/Zn^{2+} were achieved (Fig. 10**q-r**). Furthermore, the specific capacity of $MoTe_{1.7}$ reaches as high as 338 mAh g^{-1} at 0.2 A g^{-1} and exhibits a high extraordinary cycling stability of over 96 % after 10,000 cycles at 1 A g^{-1}, which is superior to many reported works (Fig. 10**s-t**). Notably, the higher capacity and cycling stability can be attributed to the highly reversible conversion reaction of $MoTe_{1.7} + nZn^{2+} + 2ne^- \leftrightarrow MoTe_{1.7-n} + nZnTe$, which is also a two steps process, similar to CuS. The above works indisputably confirm the important effects of facet/layer spacing (channels for Zn^{2+} insertion/extraction) and lattice defects on the electrochemical performance.

Complex compound materials have a layered structure similar to chalcogenide-containing inorganic materials, the performance of which is tuned by introducing larger-sized groups and atoms. By introducing larger-sized groups and atoms up to a certain content, the electrochemical performance can be greatly promoted. Some reported works are based on bismuth-based compounds. In a typical work, it has been found that the halogen atom in BiOX (X = Cl, Br, I) results in a gradually enlarged $[Bi_2O_2]^{2+}$layer distance, which are 7.38, 8.88, and 9.76 Å for BiOCl, BiOBr, and BiOI, respectively that is larger than many layered chalcogenide-containing inorganic materials [123]. Furthermore, for the X– layers distance, BiOI has the largest distance of 3.48 Å compared to the BiOCl (2.42 Å) and BiOBr (2.87 Å). And the Zn^{2+} diffusion barrier in BiOI is much lower (0.57 eV) than that of the BiOCl (1.06 eV) and BiOBr (1.42 eV). The BiOX (X = Cl, Br, I) exhibited a Zn^{2+} insertion potential of 0.39 V and a specific capacity of 253/171 mAh g^{-1} (0.1/10 A g^{-1}). Very recently, a polyanionic insertion anode ($Ti_2O(PO_4)_2{\cdot}2H_2O$)

with a lattice spacing of 0.935 nm, endowing fast and reversible insertion/extraction of Zn^{2+}, which displays an extremely low insertion potential of 0.07 V and a reversible specific capacity of 124.6 mAh g^{-1} at a current density of 50 mA g^{-1}. Furthermore, such $Ti_2O(PO_4)_2{\cdot}2H_2O$ electrode possesses an extraordinary cycling stability of 100 % after 5000 cycles (1000 mA g^{-1}) [121].

Based on the fundamental properties of inorganic intercalation anode materials, it has been determined that interlayer spacing or lattice tunnels are essential for the storage and release of Zn, which inherently leads to slow solid-state diffusion kinetics. The repeated intercalation and deintercalation of Zn^{2+} ions can easily disrupt the ion transport channels within these materials. Consequently, such inorganic anodes

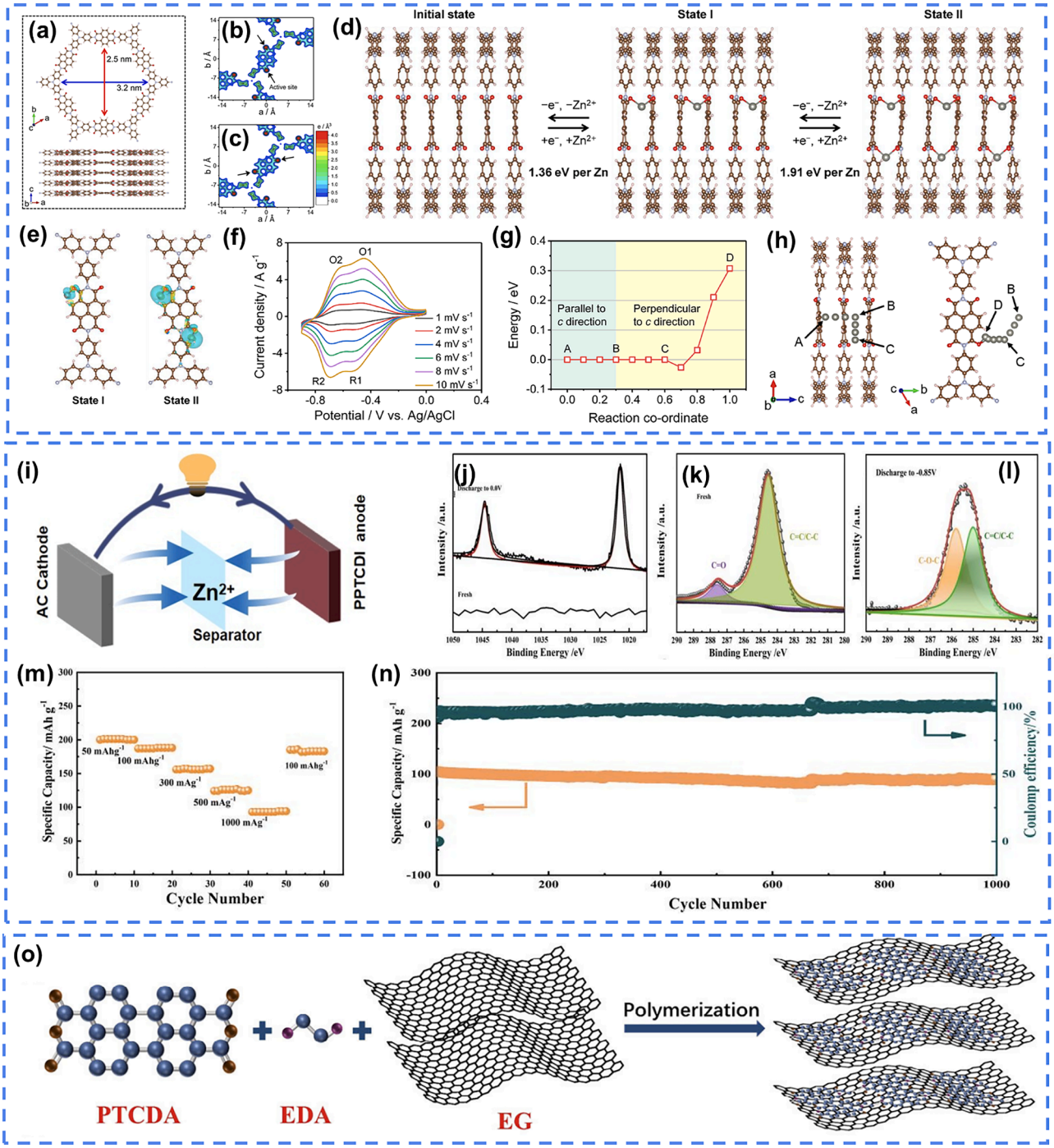

Fig. 11. (a) Top and side views of the PI-COF. Calculated electron densities of PI-COF in planes (b) 1 Å below and (c) 1 Å above the layer center. (d) Calculated Zn^{2+}-storage mechanism of PI-COF. (e) The charge-density difference of PI-COF in State I and State II. Yellow and blue regions represent the accumulation and depletion of electrons, respectively. (f) CV curves of the PI-COF electrode at different scan rates in 2 M $ZnSO_4$. (g) Energy barrier for Zn^{2+} diffusion along different directions in PI-COF, and the bonding energy with carbonyl O (from C to D). (h) Top and side views of Zn^{2+} diffusion (A → B), in the pore (B → C), and approaching active sites of PI-COF (C → D). Reprinted with permission from Ref. [108]. Copyright (2020) American Chemical Society. (i) Schematic illustration of PPTCDI intercalation anode for ZIBs. (j-l) XPS patterns of PPTCDI under different conditions. (m) Rate performance and (n) cycling stability of PPTCDI intercalation anode. Reprinted with permission from Ref. [20]. Copyright (2023) American Chemical Society. (o) Schematic illustration of PDI-EDA/EG composite preparation. Reprinted with permission from Ref. [130]. Copyright (2023) Multidisciplinary Digital Publishing Institute.

are plagued by subpar rate performance and cycling stability. Furthermore, the specific capacity of inorganic intercalation anode materials is considerably lower than that of metallic zinc, failing to satisfy commercial demands.

3.3.2. Organic materials

Even though the research of ZIBs intercalated anodes is limited to inorganic chalcogenide-based materials, organic materials are an alternative to anodes of ZIBs because of their abundant redox-active group, for example, quinone O, pyrazine N, and hexaazatrinaphthalene N [127–129], which the inorganic materials don't have. The Zn^{2+} storage in organic is achieved by reacting with the active groups to form radical anions or coordinating with cations, which would not result in huge structural deformation caused by the excessive insertion of Zn^{2+} into the facet/layer spacing [108]. Furthermore, the organic materials for ZIBs anode have relativity low toxicity, lower price, and abundant raw materials, which ensures sufficient supplies for large-scale production [20]. Therefore, developing organics-based intercalated anodes for ZIBs with sufficient redox functional groups as well as ions diffusion channels is the research priority.

In recent work, the imide C = O in PTCDI was confirmed as the redox-active site for ZIBs. For the discharge process, the carbonyl groups are reduced by capturing electrons, and at the same solid-liquid phase interface (Zn(H)–PTCDI) is formed through the H^+ and Zn^{2+} migration to the PTCDI. Afterward, the protons in Zn(H)–PTCDI were released to form Zn-PTCDI [29]. Therefore, in the aqueous electrolyte, the water protons can also act as the charge carrier. Inspired by the active PTCDI, another work periodically organized an imide-linked two-dimensional polyarylimide covalent organic framework (PI-COF) on a conductive substrate (CNTs decorated carbon cloth) as shown in Fig. 11**a** [108]. The designed crystalline PI-COF possesses a hexagonal nanochannel of 2.5 to 3.2 nm (Fig. 11**a**), which not only provides enough space for boosting Zn^{2+} diffusion but also enhances the electron conduction property. The theoretical calculations reveal the carbonyl groups in the PI-COF structure are the redox-active functional groups for ZIBs (Fig. 11**b-c**). The storage of Zn^{2+}in PI-COF is attributed to the capture and release of $Zn^{2+,}$ which is different from the organic PTCDI [108]. The Zn^{2+} gradually binds with the carbonyl O in PI-COF by overcoming two different energy barriers of 1.36 eV and 1.91 eV (Fig. 11**d**), respectively, where no H^+ participates in the energy storage process. Such a two-step storage process is well confirmed by the two pairs of redox peaks in CV curves (Fig. 11**f**). After Zn^{2+} binds to the carbonyl groups, charge accumulates around them, resulting in negatively charged enolates (Fig. 11**e**). For the calculated diffusion of the 1D structure of PI-COF (Fig. 11**g-h**), the Zn^{2+} diffusion to the active sites via the A→B (parallel to the c-axis) and B→C (perpendicular to the c-axis) pathway is zero, indicating the free migration of Zn^{2+} in the nanopores of PI-COF. Furthermore, the lowest energy barrier of Zn^{2+} transportation to the active carbonyl O is 0.3 eV (C→D pathway). The purposely designed PI-COF with large size pore channels ensures a high ions accessibility for Zn^{2+} migration with a low energy barrier and facilitates reaction with redox-active carbonyl O, which renders a specific capacity of 92 mAh g^{-1}at 0.7 A g^{-1} and a high-rate performance of 79.8 % at 7 A g^{-1}, and a long cycling stability of 85 % over 4000cycles. Very recently, in another work as shown in Fig. 11**i-l**, when using PPTCDI (which contains carbonyl O, C = O) prepared by the polymerization of PTCDA and ethylene diamine (EDA) as the intercalated anode for ZIBs, the enolate ions (C—O) were found in the discharged electrode while the carbonyl O (C = O) disappeared, which demonstrates the Zn^{2+} selectively react with C = O to generate C—O (actually, it is C − O−Zn) during the charging process [20]. This PPTCDI electrode exhibits a high specific capacity of 199.1 mAh g^{-1} (50 mA g^{-1}) and 93 mAh g^{-1} (1000 mA g^{-1}), Fig. 11**m**. Furthermore, even after 1000 cycles at a current density of 1000 mA g^{-1}, the capacity of the PPTCDI electrode can remain at 93 mAh g^{-1} (capacity retention = 95.6 %), demonstrating the extraordinary cycling stability (1 M $ZnSO_4$, Fig. 11**n**). The conductive graphene can be introduced to PDI-EDA polymer (in other words, it is PPTCDI) as a host via the π–π stacking, which can facilitate the ion/electron transfer, as shown in Fig. 11**o**. [130]. Such composite electrode exhibits enhanced rate capability retention of 81.6 % (from 0.1 A g^{-1} to 5 A g^{-1}), and excellent cycling stability of 93.4 % after 1000 cycles at a current density of 1 A g^{-1}. The organic intercalated anodes show great potential for ZIBs, however, few works are reported and need further exploration. Nowadays, organics-based intercalated anode materials are faced with low specific capacity and limited cycling stability which needs to be addressed timely.

Similar to the inorganic intercalation materials, organic intercalation anode materials also exhibit certain limitations. The distinction lies in the storage mechanism of cations within organic materials, which involves the reaction of Zn^{2+} with redox-active groups leading to the formation of radical anions and their subsequent coordination with cations, as different from the direct insertion of Zn^{2+}. [108,133,134] While structural damage to organic materials may be negligible, this storage mechanism introduces a novel challenge: the majority of organic materials reported for Zn^{2+} storage exhibit high redox potentials (greater than 1 V vs Zn^{2+}/Zn), positioning them as prospective cathode materials rather than anodes [108]. Finally, the organic intercalation materials also suffer from weak electro-conductivity, which may consequently diminish their specific capacities.

4. Summary and outlook

Rechargeable zinc-ion batteries (ZIBs) have garnered significant attention because of their enhanced safety features, simplified operational protocols, abundant resources, and cost-effective nature. Although ZIBs are attractive energy storage candidates to replace the dominant position of lithium-ion batteries, the stability of the zinc metal and the low capacity of intercalated anode materials for ZIBs undoubtedly impede commercial production, which leads to a great challenge for further exploration. Zinc metal-based anodes for ZIBs are faced with zinc dendrite growth, HER, and corrosion, which severely hinder the performance of ZIBs. Zinc dendrite growth is the most prominent problem that is harmful to the ZIBs' lifespan. The generated zinc dendrites are easily peeled from the zinc anode to result in "dead zinc", which lowers the maximum capacity of the zinc anode. In addition, the zinc dendrites can easily pierce the membranes to trigger short circuits, which disable the batteries instantly. Furthermore, the active zinc metal in mild electrolytes is prone to react with the electrolyte to generate hydrogen gas (H_2). Excess production of H_2 can rapidly increase the inner pressure of a sealed battery, which can lead to increased internal resistance and electrolyte leakage. The corrosion of the zinc metal anode is accompanied by the growth of zinc dendrites and HER. Although the corrosion of zinc can not directly disable the ZIBs due to the inherent resistance of zinc, the performance of ZIBs also gradually reduces as corrosion intensifies. Currently, a lot of research has been carried out to address these problems. However, the task of using protective coating layers on zinc surfaces to improve the ZIB anode issues remains challenging because of the lack of a thorough understanding of zinc growth. For example, the insulating and passivated ZnO coating layer on the zinc surface would increase the electrical resistance and reduce the CE of plating/stripping. Conversely, ZnO can also reduce the desolvation barrier and possesses good zincophilic characteristics, which is beneficial to uniform zinc deposition. Thus, a full understanding of different protective coating layers on zinc surfaces is very important. In this review, we fully summarized the typical protective coating layers materials, including the inorganic metal/nonmetal compounds, organic molecules, 2D carbon-based materials, 2D Mxene-based materials, and alloys.

To completely avoid the zinc dendrites growth of a zinc metal anode, the intercalated anode materials are also explored as the anode for ZIBs due to the lack of zinc source in the intercalated materials. The storage mechanism of the intercalated anode materials via the intercalation/

deintercalation of Zn^2 is different from the zinc metal anode. Because of the intercalation/deintercalation mechanism of intercalated materials, the layered structure of which is significant to the storage performance. However, currently, the exploration of intercalated anode materials for ZIBs is severely limited and the convincing Zn^{2+} storage mechanism is still far from clarification, which presents a great challenge to develop intercalated anodes with high capacity and high energy density.

Based on the summarized latest achievements of the protective coating layers on zinc surface and intercalated anode materials, we propose several viewpoints and potential suggestions for the future exploration of improved anode materials for ZIBs.

(1) The application of protective coating layers on the surface of zinc yields positive outcomes for enhancing the performance of the zinc anode by preventing direct contact between the zinc and electrolyte which induces uniform zinc deposition. However, not all the layers are beneficial to the improvement of the zinc anode. It has proved that coating layers with exclusive ions, rather than electron, conduction characteristics can facilitate the deposition of Zn ions between the anode and the coating layer rather than between the coating layer and electrolyte, the former of which is conducive to uniform zinc deposition. In addition, a low Zn^{2+} conduction of a coating layer may induce low area capacity and depth of discharge (DOD) of the Zn anodes. Consequently, an excellent Zn^{2+} diffusion within the protective coating layer is very important.
(2) Currently, the protective coating layers on zinc surfaces are widely explored and exhibit great potential in avoiding zinc dendrite growth. However, most of the coating layers are physically deposited on the zinc surface without tight bonding to the zinc substrate and are fragile which can be easily peeled off due to the huge volume change during the zinc plating/stripping process. Therefore, the in-situ construction strategies for example electrodeposition and chemical bonding on zinc surface are preferable. For example, in-situ electrodepositing alloys on zinc surfaces endow the coating layers with better mechanical properties.
(3) The protective coating layers do improve the performance of the zinc anode by suppressing the zinc dendrites growth, HER, and corrosion. Corrosion of zinc is relatively easier to overcome compared to the zinc dendrites growth and HER due to the separation of protective coating layers. In general, a coating layer with a larger specific surface area can offer more zinc nucleation and room for zinc deposition. However, it also indicates more sites may be used for HER. Thus, the micro-surface of a coating layer should possess excellent zincophilicity for zinc deposition while passivation to HER, which indicates a comprehensive consideration of designing an effective coating layer is necessary. For example, constructing an effective protective layer with zincophilic groups (Sulfo, hydroxyl, and N-acetylamino groups) and inert metals (Cu, Ag) may be effective.
(4) Lots of works claimed their protective coating layers can optimize the ion diffusion, concentration gradient, and electric field distribution. However, those problems are always explained using DFT calculations, direct evidence is still lacking. More advanced techniques should be developed to monitor those changes. In addition, an in-situ optical microscope has been widely employed to observe the zinc dendritic growth during the zinc plating process. However, the dissociation of the zinc anode during the stripping process is missing. Thus, more in situ characterization techniques including the in-situ XRD, XPS, optical microscope, FTIR, etc. should be used to explore the zinc stripping/plating process and corresponding reactions on the surface of the protective coating layer.
(5) The host materials for ZIBs anodes can significantly enhance the depth of discharge (DOD), mitigate zinc dendrite growth, and prevent corrosion due to the elimination of zinc sheets and the intentional design of 3D, porous, and ordered micro/nanostructures. However, these unique features may lead to more exposed active sites that catalyze the HER, potentially increasing the risk of internal pressure in ZIBs. Additionally, while zinc dendrites can be induced to grow horizontally on 2D graphene due to the similar lattice constants of $[0002]_{Zn}$ and $[0002]_{Graphene}$, large-scale epitaxial growth of defect-free graphene on stainless steel remains a significant challenge. Therefore, the deliberate design of host materials for ZIBs anodes should incorporate sufficient zincophilic sites and highly ordered micro/nano-structures to ensure uniform zinc deposition within the host materials. Simultaneously, it is crucial to minimize active sites that facilitate hydrogen generation. On the other hand, most host materials are applied to non-zinc substrates using a doctor blade coating technique, which may not ensure robust adhesion between the host materials and conductive substrates. This limitation could lead to the delamination of the host material layers from the conductive substrates after repeated zinc plating/stripping cycles, thereby diminishing the overall performance of ZIBs. Consequently, a surface pre-treatment of the conductive substrates is essential, or alternatively, the development of host materials with inherent excellent conductivity and mechanical performance that can serve directly as electrodes is warranted.
(6) The intercalated anode materials for ZIBs can effectively avoid the main three problems that the zinc anodes are faced with due to the absence of zinc metal within the materials. The Zn^{2+} storage for the intercalated anode materials relies on the insertion of Zn^{2+} into the layer structure and the reaction between Zn^{2+} and redox-active groups. Thus, the kinetic of Zn^{2+} is always slow. In addition, many intercalated materials are not well conductive, have low energy density, and experience material dissolution in the electrolyte. Furthermore, the periodic insertion/extraction of Zn^{2+} of intercalated materials would result in structural collapse. Worse still, the storage mechanisms of most intercalated materials are unclear and the variety of intercalated materials is also very limited. Therefore, it is of great significance to develop intercalated anode materials with good conductivity and larger layer spacing to enhance the storage capacity. Using advanced techniques such as *in-situ* XPS, XRD, SEM, and TEM to explore the storage mechanisms. For example, active layered materials can be combined with conductive carbons like CNTs and graphene to boost conductivity. Larger radius atoms or organic molecules can also serve as dopants or connectors to effectively increase the layer spacing or create extensive ion tunnels.

CRediT authorship contribution statement

Ao Yu: Writing – original draft. **Wei Zhang:** Writing – review & editing. **Nimanyu Joshi:** Writing – review & editing. **Yang Yang:** Supervision, Funding acquisition, Project administration.

Declaration of Competing Interest

We declare that we have no financial and personal relationships with other people or organizations that can inappropriately influence our work, and there is no professional or other personal interest of any nature or kind in any product, service, and/or company that could be construed as influencing the position presented in, or the review of, the manuscript entitled.

Acknowledgments

Y.Y. acknowledges financial support from the National Science Foundation under Grant No. CBET-1949840 and ACS PRF (65481-ND10). A.Y. acknowledges financial support from the Preeminent

Postdoctoral Program (P3) at UCF.

Supplementary materials

Supplementary material associated with this article can be found, in the online version, at doi:10.1016/j.ensm.2023.103075.

References

[1] J. Yang, B. Yin, Y. Sun, H. Pan, W. Sun, B. Jia, S. Zhang, T. Ma, Zinc anode for mild aqueous zinc-ion batteries: challenges, strategies, and perspectives, Nano-Micro Lett. 14 (2022) 42.

[2] J. Wang, Y. Yang, Y. Zhang, Y. Li, R. Sun, Z. Wang, H. Wang, Strategies towards the challenges of zinc metal anode in rechargeable aqueous zinc ion batteries, Energy Stor. Mater. 35 (2021) 19–46.

[3] C. Xu, B. Li, H. Du, F. Kang, Energetic zinc ion chemistry: the rechargeable zinc ion battery, Angew. Chem. Int. Ed. 51 (2012) 933–935.

[4] D. Qiu, B. Li, C. Zhao, J. Dang, G. Chen, H. Qiu, H. Miao, A review on zinc electrodes in alkaline electrolyte: current challenges and optimization strategies, Energy Stor. Mater. 61 (2023), 102903.

[5] C. Xia, J. Guo, P. Li, X. Zhang, H.N. Alshareef, Highly ode, Angew. Chem. Int. Ed. 57 (2018) 3943–3948.

[6] X. Chen, B. Liu, C. Zhong, Z. Liu, J. Liu, L. Ma, Y. Deng, X. Han, T. Wu, W. Hu, J. Lu, Ultrathin Co_3O_4 Layers with Large Contact Area on Carbon Fibers as High-Performance Electrode for Flexible Zinc–Air Battery Integrated with Flexible Display, Adv. Energy Mater. 7 (2017), 1700779.

[7] T. Yamamoto, T. Shoji, Rechargeable Zn|$ZnSO_4$|MnO_2-type cells, Inorganica Chim. Acta 117 (1986) L27–L28.

[8] Q. Li, X. Rui, D. Chen, Y. Feng, N. Xiao, L. Gan, Q. Zhang, Y. Yu, S. Huang, A high-capacity ammonium vanadate cathode for zinc-ion battery, Nano-Micro Lett. 12 (2020) 67.

[9] T. Wang, C. Li, X. Xie, B. Lu, Z. He, S. Liang, J. Zhou, Anode materials for aqueous zinc ion batteries: mechanisms, properties, and perspectives, ACS Nano 14 (2020) 16321–16347.

[10] Y. Cui, Q. Zhao, X. Wu, X. Chen, J. Yang, Y. Wang, R. Qin, S. Ding, Y. Song, J. Wu, K. Yang, Z. Wang, Z. Mei, Z. Song, H. Wu, Z. Jiang, G. Qian, L. Yang, F. Pan, An interface-bridged organic–inorganic layer that suppresses dendrite formation and side reactions for ultra-long-life aqueous zinc metal anodes, Angew. Chem. Int. Ed. 59 (2020) 16594–16601.

[11] Y. Zhang, J.D. Howe, S. Ben-Yoseph, Y. Wu, N. Liu, Unveiling the origin of alloy-seeded and nondendritic growth of Zn for rechargeable aqueous Zn batteries, ACS Energy Lett. 6 (2021) 404–412.

[12] H. Tian, G. Feng, Q. Wang, Z. Li, W. Zhang, M. Lucero, Z. Feng, Z.-L. Wang, Y. Zhang, C. Zhen, M. Gu, X. Shan, Y. Yang, Three-dimensional Zn-based alloys for dendrite-free aqueous Zn battery in dual-cation electrolytes, Nat. Commun. 13 (2022) 7922.

[13] Z. Yi, G. Chen, F. Hou, L. Wang, J. Liang, Strategies for the stabilization of Zn metal anodes for Zn-ion batteries, Adv. Energy Mater. 11 (2021), 2003065.

[14] R. Zhang, X.-B. Cheng, C.-Z. Zhao, H.-J. Peng, J.-L. Shi, J.-Q. Huang, J. Wang, F. Wei, Q. Zhang, Conductive nanostructured scaffolds render low local current density to inhibit lithium dendrite growth, Adv. Mater. 28 (2016) 2155–2162.

[15] H. Zhang, R. Guo, S. Li, C. Liu, H. Li, G. Zou, J. Hu, H. Hou, X. Ji, Graphene quantum dots enable dendrite-free zinc ion battery, Nano Energy 92 (2022), 106752.

[16] J. Cao, C. Chen, Q. Zhao, N. Zhang, Q. Lu, X. Wang, Z. Niu, J. Chen, A flexible nanostructured paper of a reduced graphene oxide–sulfur composite for high-performance lithium–sulfur batteries with unconventional configurations, Adv. Mater. 28 (2016) 9629–9636.

[17] Y. Zhang, S. Bi, Z. Niu, W. Zhou, S. Xie, Design of Zn anode protection materials for mild aqueous Zn-ion batteries, Energy Mater. 2 (2022), 200012.

[18] Y. Cheng, L. Luo, L. Zhong, J. Chen, B. Li, W. Wang, S.X. Mao, C. Wang, V. L. Sprenkle, G. Li, J. Liu, Highly reversible zinc-ion intercalation into chevrel phase Mo6S8 nanocubes and applications for advanced zinc-ion batteries, ACS Appl. Mater. Interfaces 8 (2016) 13673–13677.

[19] A.L. Jadhav, T.R. Juran, M.A. Kim, A.M. Bruck, B.E. Hawkins, J.W. Gallaway, M. Smeu, R.J. Messinger, Reversible electrochemical anionic redox in rechargeable multivalent-ion batteries, J. Am. Chem. Soc. 145 (2023) 15816–15826.

[20] R. Cang, K. Ye, K. Zhu, D. Cao, Environmentally friendly and flexible aqueous zinc ion batteries using an organic anode and activated carbon as the cathode, ACS Sustain. Chem. Eng. 11 (2023) 5065–5071.

[21] Q. Yang, G. Liang, Y. Guo, Z. Liu, B. Yan, D. Wang, Z. Huang, X. Li, J. Fan, C. Zhi, Do zinc dendrites exist in neutral zinc batteries: a developed electrohealing strategy to in situ rescue in-service batteries, Adv. Mater. 31 (2019), 1903778.

[22] Y. Liu, X. Xu, M. Sadd, O.O. Kapitanova, V.A. Krivchenko, J. Ban, J. Wang, X. Jiao, Z. Song, J. Song, S. Xiong, A. Matic, Insight into the critical role of exchange current density on electrodeposition behavior of lithium metal, Adv. Sci. 8 (2021), 2003301.

[23] Y. Zuo, K. Wang, P. Pei, M. Wei, X. Liu, Y. Xiao, P. Zhang, Zinc dendrite growth and inhibition strategies, Mater. Today Energy 20 (2021), 100692.

[24] J. Zheng, Q. Zhao, T. Tang, J. Yin, C.D. Quilty, G.D. Renderos, X. Liu, Y. Deng, L. Wang, D.C. Bock, C. Jaye, D. Zhang, E.S. Takeuchi, K.J. Takeuchi, A. C. Marschilok, L.A. Archer, Reversible epitaxial electrodeposition of metals in battery anodes, Science 366 (2019) 645–648.

[25] C.-Y. Jung, T.-H. Kim, W.-J. Kim, S.-C. Yi, Computational analysis of the zinc utilization in the primary zinc-air batteries, Energy 102 (2016) 694–704.

[26] N. Diomidis, J.P. Celis, Anodic film formation on zinc in alkaline electrolytes containing silicate and tetraborate ions, J. Electrochem. Soc. 154 (2007) C711.

[27] P. Gu, M. Zheng, Q. Zhao, X. Xiao, H. Xue, H. Pang, Rechargeable zinc–air batteries: a promising way to green energy, J. Mater. Chem. A 5 (2017) 7651–7666.

[28] M.C.H. McKubre, D.D. Macdonald, The dissolution and passivation of zinc in concentrated aqueous hydroxide, J. Electrochem. Soc. 128 (1981) 524.

[29] N. Liu, X. Wu, Y. Zhang, Y. Yin, C. Sun, Y. Mao, L. Fan, N. Zhang, Building high rate capability and ultrastable dendrite-free organic anode for rechargeable aqueous zinc batteries, Adv. Sci. 7 (2020), 2000146.

[30] Y. Tian, Y. An, C. Wei, B. Xi, S. Xiong, J. Feng, Y. Qian, Recent advances and perspectives of Zn-metal free “rocking-chair”-type Zn-ion batteries, Adv. Energy Mater. 11 (2021), 2002529.

[31] H. Liu, J.-G. Wang, Z. You, C. Wei, F. Kang, B. Wei, Rechargeable aqueous zinc-ion batteries: mechanism, design strategies and future perspectives, Mater. Today 42 (2021) 73–98.

[32] L. Yuan, J. Hao, C.-C. Kao, C. Wu, H.-K. Liu, S.-X. Dou, S.-Z. Qiao, Regulation methods for the Zn/electrolyte interphase and the effectiveness evaluation in aqueous Zn-ion batteries, Energy Environ. Sci. 14 (2021) 5669–5689.

[33] X. Luo, Q. Nian, Z. Wang, B.-Q. Xiong, S. Chen, Y. Li, X. Ren, Building a seamless water-sieving MOF-based interphase for highly reversible Zn metal anodes, Chem. Eng. J. 455 (2023), 140510.

[34] M. Qiu, H. Jia, C. Lan, H. Liu, S. Fu, An enhanced kinetics and ultra-stable zinc electrode by functionalized boron nitride intermediate layer engineering, Energy Stor. Mater. 45 (2022) 1175–1182.

[35] J. Hao, J. Long, B. Li, X. Li, S. Zhang, F. Yang, X. Zeng, Z. Yang, W.K. Pang, Z. Guo, Toward high-performance hybrid Zn-based batteries via deeply understanding their mechanism and using electrolyte additive, Adv. Funct. Mater. 29 (2019), 1903605.

[36] C. Chao, M. Man, X. Wang, Y. Wu, F. Zhang, M. Wu, Q. Xiang, Z. Luo, Y. Sun, Stable and dendrite-free Zn anode enabled by a PEDOT:PSS layer for high-performance Zn-ion capacitors, Ind. Eng. Chem. Res. 62 (2023) 1350–1357.

[37] Q. Yang, Y. Guo, B. Yan, C. Wang, Z. Liu, Z. Huang, Y. Wang, Y. Li, H. Li, L. Song, J. Fan, C. Zhi, Hydrogen-substituted graphdiyne ion tunnels directing concentration redistribution for commercial-grade dendrite-free zinc anodes, Adv. Mater. 32 (2020), 2001755.

[38] L. Kang, M. Cui, F. Jiang, Y. Gao, H. Luo, J. Liu, W. Liang, C. Zhi, Nanoporous $CaCO_3$ coatings enabled uniform Zn stripping/plating for long-life zinc rechargeable aqueous batteries, Adv. Energy Mater. 8 (2018), 1801090.

[39] H. He, H. Tong, X. Song, X. Song, J. Liu, Highly stable Zn metal anodes enabled by atomic layer deposited Al_2O_3 coating for aqueous zinc-ion batteries, J. Mater. Chem. A 8 (2020) 7836–7846.

[40] H. Liu, J.-G. Wang, W. Hua, H. Sun, Y. Huyan, S. Tian, Z. Hou, J. Yang, C. Wei, F. Kang, Building ohmic contact interfaces toward ultrastable Zn metal anodes, Adv. Sci. 8 (2021), 2102612.

[41] K. Wu, J. Yi, X. Liu, Y. Sun, J. Cui, Y. Xie, Y. Liu, Y. Xia, J. Zhang, Regulating Zn deposition via an artificial solid–electrolyte interface with aligned dipoles for long life Zn anode, Nano-Micro Lett. 13 (2021) 79.

[42] K. Zhao, C. Wang, Y. Yu, M. Yan, Q. Wei, P. He, Y. Dong, Z. Zhang, X. Wang, L. Mai, Ultrathin surface coating enables stabilized zinc metal anode, Adv. Mater. Interfaces 5 (2018), 1800848.

[43] P. Liang, J. Yi, X. Liu, K. Wu, Z. Wang, J. Cui, Y. Liu, Y. Wang, Y. Xia, J. Zhang, Highly reversible Zn anode enabled by controllable formation of nucleation sites for Zn-based batteries, Adv. Funct. Mater. 30 (2020), 1908528.

[44] J. Hao, B. Li, X. Li, X. Zeng, S. Zhang, F. Yang, S. Liu, D. Li, C. Wu, Z. Guo, An in-depth study of Zn metal surface chemistry for advanced aqueous Zn-Ion batteries, Adv. Mater. 32 (2020), 2003021.

[45] D. Wang, D. Lv, H. Peng, N. Wang, H. Liu, J. Yang, Y. Qian, Site-selective adsorption on ZnF2/Ag coated Zn for advanced aqueous zinc–metal batteries at low temperature, Nano Lett. 22 (2022) 1750–1758.

[46] P. Cao, X. Zhou, A. Wei, Q. Meng, H. Ye, W. Liu, J. Tang, J. Yang, Fast-charging and ultrahigh-capacity zinc metal anode for high-performance aqueous zinc-ion batteries, Adv. Funct. Mater. 31 (2021), 2100398.

[47] W. Han, L. Xiong, M. Wang, W. Seo, Y. Liu, S. Taj Ud Din, W. Yang, G. Liu, Interface engineering via in-situ electrochemical induced ZnSe for a stabilized zinc metal anode, Chem. Eng. J. 442 (2022), 136247.

[48] Z. Cai, J. Guo, H. Yang, Y. Xu, Electrochemical properties of electrospun poly(5-cyanoindole) submicron-fibrous electrode for zinc/polymer secondary battery, J. Power Sources 279 (2015) 114–122.

[49] S. Szpak, C.J. Gabriel, The Zn - KOH system: the solution-precipitation path for anodic ZnO formation, J. Electrochem. Soc. 126 (1979) 1914.

[50] X. Xie, S. Liang, J. Gao, S. Guo, J. Guo, C. Wang, G. Xu, X. Wu, G. Chen, J. Zhou, Manipulating the ion-transfer kinetics and interface stability for high-performance zinc metal anodes, Energy Environ. Sci. 13 (2020) 503–510.

[51] W. Deng, N. Zhang, X. Wang, Hybrid interlayer enables dendrite-free and deposition-modulated zinc anodes, Chem. Eng. J. 432 (2022), 134378.

[52] C. Choi, J.B. Park, J.H. Park, S. Yu, D.-W. Kim, Simultaneous manipulation of electron/Zn_{2+} ion flux and desolvation effect enabled by in-situ built ultra-thin oxide-based artificial interphase for controlled deposition of zinc metal anodes, Chem. Eng. J. 456 (2023), 141015.

[53] H. Peng, X. Wang, Z. Liu, H. Lei, S. Cui, X. Xie, Y. Hu, G. Ma, Alleviating Zn dendrites by growth of ultrafine ZnO nanowire arrays through horizontal

anodizing for high-capacity, long-life Zn Ion capacitors, ACS Appl. Mater. Interfaces 15 (2023) 4071–4080.
[54] C. Ma, K. Yang, S. Zhao, Y. Xie, C. Liu, N. Chen, C. Wang, D. Wang, D. Zhang, Z. X. Shen, F. Du, Recyclable and ultrafast fabrication of zinc oxide interface layer enabling highly reversible dendrite-free Zn anode, ACS Energy Lett. 8 (2023) 1201–1208.
[55] P. Sun, L. Ma, W. Zhou, M. Qiu, Z. Wang, D. Chao, W. Mai, Simultaneous regulation on solvation shell and electrode interface for dendrite-free Zn ion batteries achieved by a low-cost glucose additive, Angew. Chem. Int. Ed. 60 (2021) 18247–18255.
[56] C. Yan, H.-R. Li, X. Chen, X.-Q. Zhang, X.-B. Cheng, R. Xu, J.-Q. Huang, Q. Zhang, Regulating the inner helmholtz plane for stable solid electrolyte interphase on lithium metal anodes, J. Am. Chem. Soc. 141 (2019) 9422–9429.
[57] H. Zhang, Y. Wu, J. Yu, T. Jiang, M. Wu, Shooting three birds with one stone: the regulation of Zn2+, H2O, and OH, kinetics for stable Zn-metal anodes with a multifunctional sieve, Adv. Funct. Mater. (2023) 2301912.
[58] N. Li, Q. Ye, K. Zhang, H. Yan, C. Shen, B. Wei, K. Xie, Normalized Lithium Growth from the Nucleation Stage for Dendrite-Free Lithium Metal Anodes, Angew. Chem. Int. Ed. 58 (2019) 18246–18251.
[59] H. Liu, Q. Ye, D. Lei, Z. Hou, W. Hua, Y. Huyan, N. Li, C. Wei, F. Kang, J.-G. Wang, Molecular brush: an ion-redistributor to homogenize fast Zn2+ flux and deposition for calendar-life Zn batteries, Energy Environ. Sci. 16 (2023) 1610–1619.
[60] H. Lu, J. Hu, X. Wei, K. Zhang, X. Xiao, J. Zhao, Q. Hu, J. Yu, G. Zhou, B. Xu, A recyclable biomass electrolyte towards green zinc-ion batteries, Nat. Commun. 14 (2023) 4435.
[61] W. Yuan, L. Zhu, Y. Zheng, W. Guo, Y. Min, J. Fan, Surface engineering with interfacial poly(glutamic acid)/MXene/aramid nanofibers protective layer for dendrite-free zinc anodes, Energy Fuels 37 (2023) 8031–8041.
[62] H. Jin, S. Dai, K. Xie, Y. Luo, K. Liu, Z. Zhu, L. Huang, L. Huang, J. Zhou, Regulating interfacial desolvation and deposition kinetics enables durable Zn anodes with ultrahigh utilization of 80%, Small 18 (2022), 2106441.
[63] M. Gopalakrishnan, S. Ganesan, M.T. Nguyen, T. Yonezawa, S. Praserthdam, R. Pornprasertsuk, S. Kheawhom, Critical roles of metal–organic frameworks in improving the Zn anode in aqueous zinc-ion batteries, Chem. Eng. J. 457 (2023), 141334.
[64] E. Kim, I. Choi, K.W. Nam, Metal–organic framework for dendrite-free anodes in aqueous rechargeable zinc batteries, Electrochim. Acta 425 (2022), 140648.
[65] S. Zhou, Y. Wang, H. Lu, Y. Zhang, C. Fu, I. Usman, Z. Liu, M. Feng, G. Fang, X. Cao, S. Liang, A. Pan, Anti-corrosive and Zn-ion-regulating composite interlayer enabling long-life Zn metal anodes, Adv. Funct. Mater. 31 (2021), 2104361.
[66] Q. Zhang, J. Luan, Y. Tang, X. Ji, H. Wang, Interfacial design of dendrite-free zinc anodes for aqueous zinc-ion batteries, Angew. Chem. Int. Ed. 59 (2020) 13180–13191.
[67] Z. Li, L. Wu, S. Dong, T. Xu, S. Li, Y. An, J. Jiang, X. Zhang, Pencil drawing stable interface for reversible and durable aqueous zinc-ion batteries, Adv. Funct. Mater. 31 (2021), 2006495.
[68] P. Liu, Z. Zhang, R. Hao, Y. Huang, W. Liu, Y. Tan, P. Li, J. Yan, K. Liu, Ultra-highly stable zinc metal anode via 3D-printed g-C_3N_4 modulating interface for long life energy storage systems, Chem. Eng. J. 403 (2021), 126425.
[69] Y. Lee, B. Ma, P. Bai, Concentration polarization and metal dendrite initiation in isolated electrolyte microchannels, Energy Environ. Sci. 13 (2020) 3504–3513.
[70] A. Pei, G. Zheng, F. Shi, Y. Li, Y. Cui, Nanoscale nucleation and growth of electrodeposited lithium metal, Nano Lett. 17 (2017) 1132–1139.
[71] F. Xie, H. Li, X. Wang, X. Zhi, D. Chao, K. Davey, S.-Z. Qiao, Mechanism for zincophilic sites on zinc-metal anode hosts in aqueous batteries, Adv. Energy Mater. 11 (2021), 2003419.
[72] R. Le Van Mao, E. Rutinduka, C. Detellier, P. Gougay, V. Hascoet, S. Tavakoliyan, S.V. Hoa, T. Matsuura, Mechanical and pore characteristics of zeolite composite membranes, J. Mater. Chem. 9 (1999) 783–788.
[73] N. Zhang, S. Huang, Z. Yuan, J. Zhu, Z. Zhao, Z. Niu, Direct self-assembly of MXene on Zn anodes for dendrite-free aqueous zinc-ion batteries, Angew. Chem. Int. Ed. 60 (2021) 2861–2865.
[74] Y. Tian, Y. An, C. Wei, B. Xi, S. Xiong, J. Feng, Y. Qian, Flexible and free-standing Ti3C2Tx MXene@Zn paper for dendrite-free aqueous zinc metal batteries and nonaqueous lithium metal batteries, ACS Nano 13 (2019) 11676–11685.
[75] C. Wei, Y. Tao, Y. An, Y. Tian, Y. Zhang, J. Feng, Y. Qian, Recent advances of emerging 2D MXene for stable and dendrite-free metal anodes, Adv. Funct. Mater. 30 (2020), 2004613.
[76] J. Gu, Q. Zhu, Y. Shi, H. Chen, D. Zhang, Z. Du, S. Yang, Single zinc atoms immobilized on MXene ($Ti_3C_2Cl_x$) layers toward dendrite-free lithium metal anodes, ACS Nano 14 (2020) 891–898.
[77] Y. Tian, Y. An, C. Liu, S. Xiong, J. Feng, Y. Qian, Reversible zinc-based anodes enabled by zincophilic antimony engineered MXene for stable and dendrite-free aqueous zinc batteries, Energy Stor. Mater. 41 (2021) 343–353.
[78] C. Sun, C. Wu, X. Gu, C. Wang, Q. Wang, Interface Engineering via $Ti_3C_2T_x$ MXene Electrolyte Additive toward Dendrite-Free Zinc Deposition, Nano-Micro Lett. 13 (2021) 89.
[79] Z. Cai, Y. Ou, J. Wang, R. Xiao, L. Fu, Z. Yuan, R. Zhan, Y. Sun, Chemically resistant Cu–Zn/Zn composite anode for long cycling aqueous batteries, Energy Stor. Mater. 27 (2020) 205–211.
[80] H. Tian, Z. Li, G. Feng, Z. Yang, D. Fox, M. Wang, H. Zhou, L. Zhai, A. Kushima, Y. Du, Z. Feng, X. Shan, Y. Yang, Stable, high-performance, dendrite-free, seawater-based aqueous batteries, Nat. Commun. 12 (2021) 237.
[81] H. Tao, Z. Hou, L. Zhang, X. Yang, L.-Z. Fan, Manipulating alloying reaction to achieve the stable and dendrite-free zinc metal anodes, Chem. Eng. J. 450 (2022), 138048.
[82] S.-B. Wang, Q. Ran, R.-Q. Yao, H. Shi, Z. Wen, M. Zhao, X.-Y. Lang, Q. Jiang, Lamella-nanostructured eutectic zinc–aluminum alloys as reversible and dendrite-free anodes for aqueous rechargeable batteries, Nat. Commun. 11 (2020) 1634.
[83] M. Fayette, H.J. Chang, I.A. Rodríguez-Pérez, X. Li, D. Reed, Electrodeposited zinc-based films as anodes for aqueous zinc batteries, ACS Appl. Mater. Interfaces 12 (2020) 42763–42772.
[84] M. Kwon, J. Lee, S. Ko, G. Lim, S.-H. Yu, J. Hong, M. Lee, Stimulating Cu–Zn alloying for compact Zn metal growth towards high energy aqueous batteries and hybrid supercapacitors, Energy Environ. Sci. 15 (2022) 2889–2899.
[85] B. Li, K. Yang, J. Ma, P. Shi, L. Chen, C. Chen, X. Hong, X. Cheng, M.-C. Tang, Y.-B. He, F. Kang, Multicomponent copper-zinc alloy layer enabling ultra-stable zinc metal anode of aqueous Zn-ion battery, Angew. Chem. Int. Ed. 61 (2022), e202212587.
[86] Q. Cao, Y. Gao, J. Pu, X. Zhao, Y. Wang, J. Chen, C. Guan, Gradient design of imprinted anode for stable Zn-ion batteries, Nat. Commun. 14 (2023) 641.
[87] L. Hong, L.-Y. Wang, Y. Wang, X. Wu, W. Huang, Y. Zhou, K.-X. Wang, J.-S. Chen, Toward hydrogen-free and dendrite-free aqueous zinc batteries: formation of zincophilic protective layer on Zn anodes, Adv. Sci. 9 (2022), 2104866.
[88] M. Cui, Y. Xiao, L. Kang, W. Du, Y. Gao, X. Sun, Y. Zhou, X. Li, H. Li, F. Jiang, C. Zhi, Quasi-isolated Au particles as heterogeneous seeds to guide uniform Zn deposition for aqueous zinc-ion batteries, ACS Appl. Energy Mater. 2 (2019) 6490–6496.
[89] M. Wang, Y. Meng, K. Li, T. Ahmad, N. Chen, Y. Xu, J. Sun, M. Chuai, X. Zheng, Y. Yuan, C. Shen, Z. Zhang, W. Chen, Toward dendrite-free and anti-corrosion Zn anodes by regulating a bismuth-based energizer, eScience 2 (2022) 509–517.
[90] C. Liu, Z. Luo, W. Deng, W. Wei, L. Chen, A. Pan, J. Ma, C. Wang, L. Zhu, L. Xie, X.-Y. Cao, J. Hu, G. Zou, H. Hou, X. Ji, Liquid alloy interlayer for aqueous zinc-ion battery, ACS Energy Lett. 6 (2021) 675–683.
[91] S. Jin, Y. Ye, Y. Niu, Y. Xu, H. Jin, J. Wang, Z. Sun, A. Cao, X. Wu, Y. Luo, H. Ji, L.-J. Wan, Solid–solution-based metal alloy phase for highly reversible lithium metal anode, J. Am. Chem. Soc. 142 (2020) 8818–8826.
[92] X. Guo, Y. Ding, L. Xue, L. Zhang, C. Zhang, J.B. Goodenough, G. Yu, A self-healing room-temperature liquid-metal anode for alkali-ion batteries, Adv. Funct. Mater. 28 (2018), 1804649.
[93] G. He, Q. Li, Y. Shen, Y. Ding, Flexible amalgam film enables stable lithium metal anodes with high capacities, Angew. Chem. Int. Ed. 58 (2019) 18466–18470.
[94] H. Chen, Z. Guo, H. Wang, W. Huang, F. Pan, Z. Wang, A liquid metal interlayer for boosted charge transfer and dendrite-free deposition toward high-performance Zn anodes, Energy Stor. Mater. 54 (2023) 563–569.
[95] L. Xue, H. Gao, Y. Li, J.B. Goodenough, Cathode dependence of liquid-alloy Na–K anodes, J. Am. Chem. Soc. 140 (2018) 3292–3298.
[96] W.J. Svirbely, S.M. Read, The thermodynamic properties of liquid ternary zinc, indium, and gallium solutions, J. Phys. Chem. 66 (1962) 658–662.
[97] W. Wang, P. Zuo, G. Yin, C. Du, H. Huo, Y. Ma, Y. Gao, A dendrite-free Ga-In-Sn-Zn solid-liquid composite anode for rechargeable zinc batteries, Energy Stor. Mater. 58 (2023) 195–203.
[98] Q. Hu, J. Hou, Y. Liu, L. Li, Q. Ran, J. Mao, X. Liu, J. Zhao, H. Pang, Modulating zinc metal reversibility by confined antifluctuator film for durable and dendrite-free zinc ion batteries, Adv. Mater. 35 (2023), 2303336.
[99] Y. Zeng, X. Zhang, R. Qin, X. Liu, P. Fang, D. Zheng, Y. Tong, X. Lu, Dendrite-free zinc deposition induced by multifunctional CNT frameworks for stable flexible Zn-ion batteries, Adv. Mater. 31 (2019), 1903675.
[100] Y. Mu, Z. Li, B.-k. Wu, H. Huang, F. Wu, Y. Chu, L. Zou, M. Yang, J. He, L. Ye, M. Han, T. Zhao, L. Zeng, 3D hierarchical graphene matrices enable stable Zn anodes for aqueous Zn batteries, Nat. Commun. 14 (2023) 4205.
[101] T. Chen, Y. Wang, Y. Yang, F. Huang, M. Zhu, B.T.W. Ang, J.M. Xue, Heterometallic seed-mediated zinc deposition on inkjet printed silver nanoparticles toward foldable and heat-resistant zinc batteries, Adv. Funct. Mater. 31 (2021), 2101607.
[102] Y. Zeng, Z. Pei, D. Luan, X.W.D. Lou, Atomically dispersed zincophilic sites in N,P-codoped carbon macroporous fibers enable efficient Zn metal anodes, J. Am. Chem. Soc. 145 (2023) 12333–12341.
[103] C. Li, Q. Shao, K. Luo, Y. Gao, W. Zhao, N. Cao, S. Du, X. Jin, P. Zou, X. Zang, A lean-zinc and zincophilic anode for highly reversible zinc metal batteries, Adv. Funct. Mater. (2023) 2305204.
[104] Z. Kang, C. Wu, L. Dong, W. Liu, J. Mou, J. Zhang, Z. Chang, B. Jiang, G. Wang, F. Kang, C. Xu, 3D porous copper skeleton supported zinc anode toward high capacity and long cycle life zinc ion batteries, ACS Sustain. Chem. Eng. 7 (2019) 3364–3371.
[105] X. Shi, G. Xu, S. Liang, C. Li, S. Guo, X. Xie, X. Ma, J. Zhou, Homogeneous deposition of zinc on three-dimensional porous copper foam as a superior zinc metal anode, ACS Sustain. Chem. Eng. 7 (2019) 17737–17746.
[106] Y. Qian, C. Meng, J. He, X. Dong, A lightweight 3D Zn@Cu nanosheets@activated carbon cloth as long-life anode with large capacity for flexible zinc ion batteries, J. Power Sources 480 (2020), 228871.
[107] G. Zhang, X. Zhang, H. Liu, J. Li, Y. Chen, H. Duan, 3D-printed multi-channel metal lattices enabling localized electric-field redistribution for dendrite-free aqueous Zn ion batteries, Adv. Energy Mater. 11 (2021), 2003927.
[108] M. Yu, N. Chandrasekhar, R.K.M. Raghupathy, K.H. Ly, H. Zhang, E. Dmitrieva, C. Liang, X. Lu, T.D. Kühne, H. Mirhosseini, I.M. Weidinger, X. Feng, A high-rate two-dimensional polyarylimide covalent organic framework anode for aqueous Zn-ion energy storage devices, J. Am. Chem. Soc. 142 (2020) 19570–19578.

[109] S. Wang, Z. Huang, X. Liu, X. Yang, R. Zhang, Monoclinic MoOx anode material synthesized by a facile N-methylpyrrolidone-assisted wet-chemical method for rechargeable aqueous zinc ion batteries, Ionics (Kiel) 28 (2022) 4283–4293.
[110] T. Xiong, Y. Zhang, Y. Wang, W.S.V. Lee, J. Xue, Hexagonal MoO_3 as a zinc intercalation anode towards zinc metal-free zinc-ion batteries, J. Mater. Chem. A 8 (2020) 9006–9012.
[111] X. Chen, R. Huang, M. Ding, H. He, F. Wang, S. Yin, Hexagonal WO_3/3D porous graphene as a novel zinc intercalation anode for aqueous zinc-ion batteries, ACS Appl. Mater. Interfaces 14 (2022) 3961–3969.
[112] Q. Lei, J. Zhang, Z. Liang, Y. Yue, Z. Ren, Y. Sun, Z. Yao, J. Li, Y. Zhao, Y. Yin, P. Huai, Z. Lv, J. Li, Z. Jiang, W. Wen, X. Li, X. Zhou, D. Zhu, Synergistic engineering of sulfur vacancies and heterointerfaces in copper sulfide anodes for aqueous Zn-Ion batteries with fast diffusion kinetics and an ultralong lifespan, Adv. Energy Mater. 12 (2022), 2200547.
[113] Z. Lv, B. Wang, M. Ye, Y. Zhang, Y. Yang, C.C. Li, Activating the stepwise intercalation–conversion reaction of layered copper sulfide toward extremely high capacity zinc-metal-free anodes for rocking-chair zinc-ion batteries, ACS Appl. Mater. Interfaces 14 (2022) 1126–1137.
[114] Z. Lv, Y. Tan, Y. Kang, J. Yang, X. Cheng, W. Meng, Y. Zhang, C.C. Li, J. Zhao, Y. Yang, Non-desolvation Zn^2 storage mechanism enables MoS2 anode with enhanced interfacial charge-transfer kinetics for low temperature zinc-ion batteries, Sci. China Chem. 66 (2023) 1537–1548.
[115] W. Li, K. Wang, S. Cheng, K. Jiang, An Ultrastable presodiated titanium disulfide anode for aqueous “rocking-chair” zinc ion battery, Adv. Energy Mater. 9 (2019), 1900993.
[116] L. Wen, Y. Wu, S. Wang, J. Shi, Q. Zhang, B. Zhao, Q. Wang, C. Zhu, Z. Liu, Y. Zheng, J. Su, Y. Gao, A novel $TiSe_2$ (de)intercalation type anode for aqueous zinc-based energy storage, Nano Energy 93 (2022), 106896.
[117] M.S. Chae, J.W. Heo, S.-C. Lim, S.-T. Hong, Electrochemical zinc-ion intercalation properties and crystal structures of $ZnMo_6S_8$ and $Zn_2Mo_6S_8$ Chevrel phases in aqueous electrolytes, Inorg. Chem. 55 (2016) 3294–3301.
[118] Y. Du, B. Zhang, W. Zhou, R. Kang, W. Zhang, H. Jin, J. Wan, J. Qin, J. Zhang, G. Chen, Laser-radiated tellurium vacancies enable high-performance telluride molybdenum anode for aqueous zinc-ion batteries, Energy Stor. Mater. 51 (2022) 29–37.
[119] Y. Du, B. Zhang, R. Kang, W. Zhou, J. Qin, J. Wan, J. Zhang, G. Chen, Practical conversion-type titanium telluride anodes for high-capacity long-lifespan rechargeable aqueous zinc batteries, J. Mater. Chem. A 10 (2022) 16976–16985.
[120] P. Cai, K. Wang, J. Ning, X. He, M. Chen, Q. Li, H. Li, M. Zhou, W. Wang, K. Jiang, Advanced in situ induced dual-mechanism heterointerface towards ultrastable aqueous rocking-chair zinc-ion batteries, Adv. Energy Mater. 12 (2022), 2202182.
[121] W. Deng, Z. Huang, Z. Zhou, C. Li, Y. Chen, Y. Zhou, C. Huang, J. Zhu, W. Zou, R. Zhu, Y. Xu, R. Li, A near 0V and low-strain intercalative anode for aqueous zinc-ion batteries, ACS Energy Lett 8 (2023) 3171–3179.
[122] Y. Qian, X. Li, H. Wang, T. Song, Y. Pei, L. Liu, X. Wang, Q. Deng, X. Wu, B. Long, $BiOIO_3$@$Zn_3(PO_4)_2{\cdot}4H_2O$ heterojunction with fast ionic diffusion kinetics for long-life “rocking-chair” zinc ion batteries, ACS Appl. Mater. Interfaces 15 (2023) 17757–17766.
[123] Q. Zhang, T. Duan, M. Xiao, Y. Pei, X. Wang, C. Zhi, X. Wu, B. Long, Y. Wu, BiOI nanopaper as a high-capacity, long-life and insertion-type anode for a flexible quasi-solid-state Zn-Ion battery, ACS Appl. Mater. Interfaces 14 (2022) 25516–25523.
[124] B. Long, Q. Zhang, T. Duan, T. Song, Y. Pei, X. Wang, C. Zhi, X. Wu, Q. Zhang, Y. Wu, Few-atomic-layered co-doped BiOBr nanosheet: free-standing anode with ultrahigh mass loading for “rocking chair” zinc-ion battery, Adv. Sci. 9 (2022), 2204087.
[125] Y. Qian, H. Wang, X. Li, T. Song, Y. Pei, L. Liu, B. Long, X. Wu, X. Wang, Sn-doped BiOCl nanosheet with synergistic H^+/Zn^{2+} co-insertion for “rocking chair” zinc-ion battery, J. Energy Chem. 81 (2023) 623–632.
[126] M. Han, Y. Qian, X. Li, N. Wang, T. Song, L. Liu, X. Wang, X. Wu, M.-K. Law, B. Long, Ni-doped $Bi_2O_2CO_3$ nanosheet with H^+/Zn^{2+} co-insertion for “rocking chair” zinc-ion battery, J. Colloid Interface Sci. 645 (2023) 483–492.
[127] R. Shi, L. Liu, Y. Lu, C. Wang, Y. Li, L. Li, Z. Yan, J. Chen, Nitrogen-rich covalent organic frameworks with multiple carbonyls for high-performance sodium batteries, Nat. Commun. 11 (2020) 178.
[128] C. Peng, G.-H. Ning, J. Su, G. Zhong, W. Tang, B. Tian, C. Su, D. Yu, L. Zu, J. Yang, M.-F. Ng, Y.-S. Hu, Y. Yang, M. Armand, K.P. Loh, Reversible multi-electron redox chemistry of π-conjugated N-containing heteroaromatic molecule-based organic cathodes, Nat. Energy 2 (2017) 17074.
[129] J. Xu, Y. He, S. Bi, M. Wang, P. Yang, D. Wu, J. Wang, F. Zhang, An olefin-linked covalent organic framework as a flexible thin-film electrode for a high-performance micro-supercapacitor, Angew. Chem. Int. Ed. 58 (2019) 12065–12069.
[130] Y. Tang, S. Li, M.-F. Lin, J. Chen, A.L.-S. Eh, Q. Xu, A π–π stacked high-performance organic anode for durable rocking-chair zinc-ion battery, Batteries 9 (2023) 318.
[131] M. Ghosh, V. Vijayakumar, M. Kurian, S. Dilwale, S. Kurungot, Naphthalene dianhydride organic anode for a ‘rocking-chair’ zinc–proton hybrid ion battery, Dalton Trans. 50 (2021) 4237–4243.
[132] B.C. Melot, J.M. Tarascon, Design and preparation of materials for advanced electrochemical storage, Acc. Chem. Res. 46 (2013) 1226–1238.
[133] W. Wang, V.S. Kale, Z. Cao, S. Kandambeth, W. Zhang, J. Ming, P.T. Parvatkar, E. Abou-Hamad, O. Shekhah, L. Cavallo, M. Eddaoudi, H.N. Alshareef, Phenanthroline covalent organic framework electrodes for high-performance zinc-ion supercapattery, ACS Energy Lett. 5 (2020) 2256–2264.
[134] M. Yu, R. Dong, X. Feng, Two-dimensional carbon-rich conjugated frameworks for electrochemical energy applications, J. Am. Chem. Soc. 142 (2020) 12903–12915.